A multifaceted cellular damage repair and prevention pathway promotes high level tolerance to β-lactam antibiotics

Jung-Ho Shin [1, 2], Donghui Choe[4, 5], Brett Ransegnola[1, 2], Hye-Rim Hong [1, 2], Ikenna Onyekwere[1, 2], Byung-Kwan Cho[4, 5, 6], and Tobias Dörr [1, 2, 3a]

[1] Weill Institute for Cell and Molecular Biology, Cornell, University, Ithaca, NY 14853, USA

[2] Department of Microbiology, Cornell University, Ithaca NY 14853, USA

[3] Cornell Institute of Host-Microbe Interactions and Disease, Cornell University, Ithaca NY 14853, USA

[4] Department of Biological Sciences, Korea Advanced Institute of Science and Technology, Daejeon 34141, Republic of Korea.

[5] KI for the BioCentury, Korea Advanced Institute of Science and Technology, Daejeon 34141, Republic of Korea.

[6] Intelligent Synthetic Biology Center, Daejeon 34141, Republic of Korea.

[a] corresponding author: tdoerr@cornell.edu

Abstract

Bactericidal antibiotics are powerful drugs due to their ability to not only inhibit essential bacterial functions, but to convert them into toxic (and potentially lethal) processes. However, many important bacterial pathogens are remarkably tolerant against bactericidal drugs, due to inducible stress responses that repair antibiotic-induced damage. The mechanistic details of how stress responses promote whole population tolerance in important human pathogens are unknown. The two-component system VxrAB of the diarrheal pathogen *Vibrio cholerae,* a model system for high-level β-lactam

tolerance, is induced by exposure to cell wall acting antibiotic and controls a gene network encoding highly diverse functions, including cell wall synthesis functions and iron uptake systems. Here, we show that positive control over cell wall synthesis functions only partially explains high level β-lactam tolerance. We find that in addition to cell wall damage, β-lactam antibiotics inappropriately induce the Fur-regulated iron starvation response, causing an increase in intracellular free iron levels and colateral oxidative damage. We propose that VxrAB reduces antibiotic-induced toxic influx of Fe^{2+} and concomitant metabolic perturbations by selectively downregulating iron uptake transporters. Our results suggest that the ability to counteract diverse antibiotic-induced stresses promotes high-level antibiotic tolerance and highlight the complex responses elicited by antibiotics in addition to their primary mechanism of action.

Introduction

The discovery and development of antibiotics is one of the most important biomedical breakthroughs in human history. The introduction of drugs that selectively kill bacteria (bactericidal antibiotics) or inhibit their growth (bacteriostatic antibiotics) has directly saved countless lives by enabling treatment of once common causes of death like pneumonia and sepsis and indirectly enabled other medical breakthroughs, including transplantation medicine and chemotherapy [1,2]. All this progress is threatened due to the rapid increase in the occurrence of antibiotic treatment failure. We urgently need to develop new therapeutics and improve the effectiveness of existing ones; this would be aided by a precise understanding of antibiotic mechanisms of action, and especially of bacterial strategies to avoid their noxious effects. In principle, bacteria resist antibiotics

by either developing the ability to grow in their presence (antibiotic resistance, ABR) or to simply stay alive in their presence for extended time periods (antibiotic tolerance/persistence) [3-8]. While the mechanisms and consequences of ABR are relatively well-established, antibiotic tolerance remains poorly understood, limiting our ability to develop antibiotic adjuvants that increase the efficacy of existing drugs.

The β-lactam antibiotics (penicillins, cephalosporins, carbapenems, cephamycins and monobactams) are highly potent bactericidal agents. Their typically lethal action results from their ability to simultaneously inhibit multiple targets (i.e, the transpeptidase domain of multiple penicillin-binding proteins [PBPs]), which ultimately causes bacterial cells to deplete essential cell wall precursors and self-destruct through the activity of endogenous, cell wall lytic enzymes ('autolysins'; endopeptidases, amidases and lytic transglycosylases) [9-12]. However, we and others have recently shown that many clinically significant Gram-negative pathogens are remarkably β-lactam tolerant. The cholera pathogen *Vibrio cholerae,* the opportunistic pathogen *Pseudomonas aeruginosa* and clinical isolates of *Enterobacteriaceae* all survive treatment with β-lactam antibiotics (including the "last resort" agent meropenem) by forming non-dividing, cell wall deficient spheroplasts [11,13,14]. Upon removal of the antibiotic, spheroplasts rapidly revert to wild-type shape and exponential growth, providing a possible explanation for treatment failure in the clinic. Spheroplasts are reminiscent of bacteria in the so-called L-form state [15,16] with the crucial distinction that spheroplasts, unlike L-forms, do not divide in the presence of antibiotics.

The extent of antibiotic tolerance is a reflection of the cell's ability to mount a stress response to counteract primary damage resulting from antibiotic-target interactions [17,18]. Numerous bacteria encode cell envelope damage response systems (alternative sigma factors and two-component response regulators) that sense damage to the cell wall or membranes and consequently upregulate complex regulons aimed at damage repair [19-25]. In *V. cholerae*, high-level β-lactam tolerance depends on the cell wall damage sensing two-component system VxrAB (also known as WigKR) [17]. The vast VxrAB regulon is induced by cell wall-acting antibiotics and includes cell wall synthesis functions and those involved in biofilm formation and type VI secretion, *inter alia* [17,26,27]. How VxrAB promotes high level tolerance against bactericidal β-lactams is unknown, but logically must rely on repair of cellular damage inflicted by β-lactam antibiotics, *i.e.*, primarily cell envelope damage. However, in addition to their primary mechanism of action, bactericidal antibiotics have also been proposed to generate toxic reactive oxygen species (ROS) as a byproduct, which are thought to enhance cell death [28-31]. This idea has been highly controversial and the resulting debate about it is ongoing [32-37]. Here, we present evidence supporting a multifactorial role for VxrAB in promoting high-level β-lactam tolerance. We have found that the ability to upregulate cell wall synthesis functions only accounts for part of the high-level tolerance observed in wild-type *V. cholerae.* In addition, we propose that VxrAB's role in promoting tolerance is to downregulate iron acquisition systems which are inappropriately induced due to the accumulation of reactive oxygen species that are produced upon exposure to penicillin. Our data highlight the pleiotropic nature of antibiotic mechanism of action and provide a

blueprint for the mechanistic underpinnings of the high-level β-lactam tolerance often observed in significant Gram-negative pathogens.

Results

ChIP-Seq and RNA-Seq reveal a complex cell wall damage response

We previously elucidated the transcriptional network controlled by VxrAB upon overexpression of a phosphomimetic version of VxrB ($VxrB^{D78E}$). Here, we directed our attention to genes directly controlled by the VxrAB response. To this end, we performed a ChIP-Seq experiment using a strain with functional, His-tagged, chromosomally encoded VxrB assayed during penicillin (PenG) treatment. After 180 min of PenG exposure (100 µg/ml, 10x MIC; these are the same conditions used in our previous study[17]), 424 putative VxrB binding events were identified by comparison with a similarly treated control strain expressing wild type, untagged VxrB (**Fig. 1A,** see **Table S3** for complete list). We then validated the ChIP-Seq results via electromobility shift assays (EMSA) of the 10 DNAs from the strongest VxrB binding events (**Fig. S1**) and, for a subset, differential regulation via S1 nuclease assays of PenG-treated cells. We then integrated this ChIP-Seq dataset with our re-analyzed (with more stringent parameters, see Methods for details) previous RNA-Seq dataset of overexpressed $VxrB^{D78E}$ [17] (**Fig. 1B,** see **Table S4** and **S5** for a complete list) to score VxrB binding events that coincided with transcriptional up- or downregulation of the associated gene(s) (**Table S5**). Our analysis resulted in the identification of 102 genes/operons that contained a putative VxrB binding site and exhibited significantly increased, VxrB-dependent expression levels, and 38 genes/operons that were scored as candidates for direct

binding and downregulation (**Table S5**). Preliminary functional assignments using the KEGG database [38] revealed that the VxrB regulon controlled a large number (76.4% 107/140) of genes of unknown function. Among the annotated upregulated genes, many coded for functions related to cell envelope biology (ABC transporters, peptidoglycan synthesis, and membrane synthesis) (**Fig. S2**). Among the downregulated genes, we observed genes encoding proteins involved in iron uptake systems, flagellar biosynthesis, carbon metabolism, chemotaxis, cell wall lytic enzymes and lipopolysaccharide biosynthesis (**Fig. S2**). Importantly, genes encoding cell wall synthesis functions (e.g. class A PBP1a [aPBP1a]), whose Vxr-dependent transcriptional regulation we have extensively validated previously [17], exhibited strong VxrB binding sites (**Fig. 1D**) and differential, Vxr-dependent regulation in S1 nuclease assays, increasing our confidence in the robustness of the ChIP-Seq dataset. Both ChIP-Seq and RNA-Seq also corroborated autoregulation of the VxrAB operon (**Fig**. **1B, Table S1**). We noted that while many of the putatively Vxr-controlled genes exhibited VxrB binding in addition to differential regulation by phosphomimetic VxrB and VxrAB-dependent regulation upon exposure to PenG (**Fig. 1D,** PBP1a and ZapB), some genes were apparently indirectly regulated as they clearly exhibited transcriptional downregulation (both upon overexpression of $VxrB^{D78E}$ and exposure to PenG) without a clear signal in our VxrB ChIP-Seq experiment (**Fig. 1D,** *flaA***)**. We speculate that this may reflect either true indirect regulation or perhaps differential binding of the phosphorylated versus the non-phosphorylated form of VxrB. Thus, the VxrAB cell wall stress response controls a gene network composed of diverse functions with an

apparent enrichment for functions required for cell envelope homeostasis and iron acquisition.

DNA footprinting analysis identifies putative VxrB binding sites

Based on an alignment of putative VxrB binding sites, we used the MEME suite [39] to identify the canonical VxrB consensus binding site ("Vxr box"). We based our analysis on the 102 upregulated and the 38 downregulated genes separately, reasoning that binding site variations may account for up- *versus* downregulation. This resulted in the putative VxrB binding motif TTGACAAAA-N2-TTGAC (N=any nucleotide) for the upregulated genes and CGCTCATTTTTTAACCAAGT for the downregulated genes. However, these putative binding motifs were poorly conserved across all Vxr-controlled genes. We hypothesize that this may be reflective of different binding characteristics of the phosphorylated vs. non-phosphorylated forms of VxrB; both forms might be expected to occur after PenG treatment and could bind to different motifs. To further characterize the VxrB binding site we conducted DNAse I footprinting assays using purified VxrB and promoter regions of putative Vxr-controlled genes (**Fig. 2AB, S3**). We again chose genes with the strongest VxrB binding as indicated in our EMSA and ChIP-Seq experiments. In 10 out of 15 promoters, VxrB protected a ~ 50 bp sequence from DNAse I digestion at low µM concentrations (**Fig. S3**), again corroborating direct binding to these promoters. However, apparent affinity varied between promoters, with the promoters of *pbp1a*, encoding aPBP1a, *mgtE*, encoding a magnesium transporter and *murJ*, encoding the lipid II flippase exhibiting the highest degree of protection (**Fig. 2AB, Fig. S3)**. Surprisingly, we were again unable to construct a well-conserved binding site

for VxrB based on this subset of promoters, despite three independent assays unequivocally demonstrating binding. This apparent binding promiscuity suggests that VxrB might have the capacity to bind to a wide range of promoter sequences *in vivo* and/or that it requires as yet unidentified accessory factors to modulate binding.

Control of cell wall synthesis only partially explains VxrAB's requirement for β-lactam tolerance

To elucidate the mechanism of β-lactam tolerance in *V. cholerae,* we sought to dissect the individual contributions of VxrB-regulated genes to resistance to killing. Since the primary mechanism of action of β-lactam antibiotics is inhibition of cell wall synthesis, we first investigated the role of Vxr-induced PG biogenesis in antibiotic tolerance. We took two approaches to eliminate VxrB's positive control over PG synthesis. For aPBP1a, we engineered a strain with a deletion in the second, functionally semi-redundant [40,41] aPBP1b, which also contains an IPTG-inducible PBP1a as its sole copy. As expected, growth of this strain was IPTG concentration-dependent (**Fig. S4**). We then grew this strain either in high concentrations of IPTG (high PBP1a levels) or very low concentrations that markedly reduced growth rate (**Fig. S4**). Addition of PenG to low aPBP cultures resulted in only a modest (5 – 10-fold) decrease in viability (**Fig. 2C**). This observation suggests that upregulation of PBP1a is indeed critical for survival in the presence of PenG, but cannot account entirely for the steep, ~10.000-fold decrease in post-antibiotic plating efficiency (**Fig. 2E** and [17]) of the Δ*vxrAB* mutant.

To corroborate these results, we also created a mutant with a partial in the putative VxrB binding site of the *murJ* gene as determined from our DNA footprinting experiment. MurJ-mediated PG precursor translocation is a critical bottleneck for cell wall synthesis [42,43]. We thus expected that introducing a mutation that removes Vxr's positive control over this step would allow us to gauge the significance of VxrB control over cell wall synthesis. S1 nuclease assays confirmed that in the VxrB binding site deletion strain, *murJ* expression was not significantly induced by PenG, similar to a Δ*vxrAB* strain (**Fig. 2D**). Similar to our observations with low PBP1a expression, the Vxr-independent *murJ* strain exhibited modest (10-fold) lethality upon exposure to PenG (**Fig. 2E**). We conclude that the ability to upregulate cell wall synthesis functions via VxrAB accounts for only some of its ability to promote tolerance.

The* VxrB *regulon controls iron acquisition systems

Based on our previous RNA-Seq data, VxrB downregulates genes involved in iron acquisition [17]. Indeed, examination of the RNA-Seq/ChIP-Seq datasets revealed a high overlap between genes regulated by VxrB with those regulated by the iron starvation response repressor Fur [44]. 47 out of the putative 63 Fur-regulated genes were also downregulated by VxrB and 20 out of these 63 genes contained both a putative VxrB and a Fur binding site (**Fig. 3AB**). Thus, the VxrB system appears to control multiple functions required for iron homeostasis. Consistent with a role in maintaining proper iron homeostasis, the Δ*vxrAB* mutant was more sensitive to growth inhibition by Fe^{2+} than the wild type strain (**Fig. S5**).

Given VxrAB's apparent role in downregulating iron acquisition in response to cell wall damage, we expected that surplus iron accumulates in a PenG-treated Δ*vxrAB* mutant and that this might be detrimental to cells under these conditions. To test this, we measured intracellular iron levels using ICP-MS during treatment with PenG. Before treatment, both WT and the Δ*vxrAB* mutant strain contained similar iron levels at ~280 ng/mg protein (**Fig. 3C)**. After 1 h of PenG exposure, WT iron levels remained relatively constant while the iron content of the Δ*vxrAB* strain started to increase significantly by ~60 % compared to baseline. Iron levels increased slightly in the WT between 90 min and 3 h, while levels in the Δ*vxrAB* mutant remained significantly higher. Consistent with an increase in free intracellular iron, the WT also became more sensitive to the iron-dependent quinone antibiotic streptonigrin [45,46] upon treatment with PenG (**Fig. 3D).** Thus, PenG exposure causes enhanced iron influx. If this iron influx is detrimental, we would expect iron chelators to alleviate the Δ*vxrAB* β-lactam sensitivity defect. Indeed, addition of 250 µM (0.25 x MIC) of the intracellular iron chelator 2,2' bipyridyl reproducibly increased survival of the Δ*vxrAB* mutant 50 – 100-fold (**Fig. 3E**); the ability to partially rescue could be reverted by addition of iron to the growth medium. As a caveat, we cannot fully exclude that the iron chelator reduces metabolic activity, and thus the rate of cell wall turnover, in a subpopulation of cells (*e.g.,* those that stochastically have lower iron levels to begin with), which could non-specifically increase tolerance levels, similar to what has been suggested before [33]. However, in conjunction with our ICP-MS/streptonigrin data demonstrating increased iron uptake in

PenG-treated cells, we tentatively interpret these data as evidence of iron-dependent toxicity in Δ*vxrAB* cells.

Penicillin exposure induces ROS defense systems, ROS and oxidative damage

Iron is thought to be toxic to cells due to its ability to convert hydrogen peroxide (a byproduct of metabolic processes) into oxygen radicals that pleiotropically oxidize and thus damage macromolecules such as proteins and DNA [47] and generally disturb metal homeostasis [48]. Indeed, antibiotics have been proposed to induce the increased production of ROS through metabolic perturbations [29,31,37], however, the extent to which this contributes to killing by antibiotics remains highly controversial [32-34]. To interrogate the potential significance of ROS to lethality of the Δ*vxrAB* mutant, we first assessed whether oxidative stress response systems were induced by PenG. We found that PenG rapidly (within ~20 min) induced members of the H_2O_2 responsive OxyR1 regulon (*prxA* and *dps*) [49-51], in the WT. Transcript levels of both OxyR1 readouts remained high initially and then decreased to below baseline after ~ 60 min (*prxA*) or 180 min (*dps)*, suggesting that the wild type strain induces a response that detoxifies hydrogen peroxide (**Fig. 4A, S6**). Both transcripts are induced by H_2O_2 in an OxyR1-dependent manner [49,50] and we validated responsiveness to hydrogen peroxide for the *prxA* transcript in our strain **(Fig. S6A).** Thus, *prxA* and *dps* are *bona fide* readouts for H_2O_2 production. Interestingly, the transcript for the response regulator OxyR1 itself was upregulated upon PenG exposure, with dynamics similar to those observed for members of its regulon (**Fig. S6B**). In the model organism *E. coli*, *oxyR* transcript levels do not change under H_2O_2 exposure [52] and our results suggest that *V. cholerae* might

employ a different mode of regulation of its oxidative stress responses. A return to baseline coincided with the upregulation of *V. cholerae*'s two catalases (*katB* and *katG*; only *katG* appears to be under OxyR1 control in the cholera pathogen [50,51]) at later stages of antibiotic exposure (**Fig. 4A**, **Fig. S6B**), likely revealing the detoxification mechanism that enables the repression of the OxyR1 regulon. Consistent with a H_2O_2 sensing function, KatG was also induced by hydrogen peroxide (**Fig. S6A**).

In the Δ*vxrAB* strain, *oxyR1* baseline levels were slightly increased compared to the wild type, while *prxA* and *dps* levels were similar. After exposure to PenG, *oxyR1* levels decreased at first but the transcript remained detectable and above the wild-type baseline for longer than the WT background (**Fig. 4A, S6**). The *prxA* and *dps* transcripts exhibited a dynamic pattern with strong induction (*dps)* or transient downregulation (*prxA*) in the mutant. We observed a pattern similar to *oxyR1* with a gene coding for another oxidative stress mitigation factor, the Alkyl hydroperoxide reductase C, *ahpC* (**Fig. S6B**). Interestingly, the transcript for *katG* remained uninduced in the *vxrAB* mutant.

We confirmed that transcriptional regulation also resulted in increased catalase protein activity using a gel-based activity assay for catalases (**Fig. 4B,** see Methods for details) after exposure to PenG. We also included an assay for SOD (**Fig. 4B**) activity, since superoxide dismutases are broadly conserved, important ROS scavenger enzymes [53]. Consistent with the observed transcript levels (**Fig. 4A**), catalases were only induced in the WT, but not the mutant (**Fig. 4C**). In contrast, SOD activity increased similarly in

both the WT and the *vxrAB* mutant (**Fig. 4D**). Taken together, these results suggest that both the WT and Δ*vxrAB* induce responses upon exposure to PenG that are associated with oxidative stress, albeit with different, complex dynamics.

Since the transcriptional response to PenG suggested that cells may experience oxidative damage, we next sought to measure ROS, and the consequences of their generation, directly. First, we used a highly sensitive, fluorimetric assay (Amplex Red) to measure intracellular hydrogen peroxide concentrations. Upon exposure to PenG, both the WT and Δ*vxrAB* mutant experienced a transient increase in hydrogen peroxide concentrations, with a peak between 20 and 60 minutes, followed by a decrease back to baseline. However, the H_2O_2 concentration in the *vxrAB* mutant was significantly elevated and at peak (20 - 60 min) accumulated more than double the concentration measured in wild type cells (**Fig. 5A**). As expected, and consistent with the accurate ability of Amplex Red to report H_2O_2, a Δ*oxR1* Δ*katB* Δ*katG* triple mutant, which lacks the ability to elaborate the primary H_2O_2 detoxification systems, exhibited both higher baseline and PenG-induced levels of H_2O_2 than the WT and Δ*vxrAB* mutant; additionally, external spiking of catalase into our assay reactions completely abolished the signal (**Fig. 5A**). We also measured H_2O_2 in the supernatant of PenG-treated cells, since H_2O_2 should be able to diffuse through membranes to some degree. We did not, however, note a meaningful accumulation of peroxide in the supernatant of any of our mutants (**Fig. 5B**), demonstrating that at least for the duration of our measurements, there was no significant diffusion out of the cell.

We next assessed the cellular consequences of oxidative damage using a protein oxidation assay via Western Blot. Consistent with our results showing enhanced iron sensitivity of the mutant, protein oxidation levels were increased in the Δ*vxrAB* mutant vs. WT even prior to addition of antibiotic (**Fig. 5C**). Addition of PenG resulted in a rapid (within 20 min) increase in protein oxidation levels in the WT, which decreased after 40 min but stayed above baseline throughout β-lactam exposure. In contrast, the *vxrAB* mutant steadily accumulated oxidized proteins throughout the exposure time, corroborating that oxidative stress has a more profound effect on the *vxrAB* mutant than the WT strain. Both, wild type and the *vxrAB* mutant exhibited increased protein oxidation when exposed to hydrogen peroxide as a positive control (**Fig. 5C, Fig. S7**). Taken together, these data suggest that both WT and Δ*vxrAB* experience oxidative stress in the presence of PenG and the Δ*vxrAB* mutant is unable to mount a sufficient response.

The electron transport chain is required for both maximal killing and **H_2O_2** ***production***

How does PenG treatment result in production of ROS? A possible origin is the electron transport chain (ETC), which in *V. cholerae* is a major generator of ROS under normal growth conditions [54]. To test the ETC's involvement in PenG-induced ROS production, we created mutants in two ETC components, namely *V. cholerae's* principal sodium translocating NADH dehydrogenase NqrA [55] and *ubiA*, which encodes a key initial step towards ubiquinone biosynthesis. NqrA has been shown to be a significant source of ROS under normal growth conditions [54], but for both mutants, we expect a drastic

reduction in ETC electron flow. Crucially, neither mutation resulted in a significantly decreased growth rate when grown in medium containing the fermentable carbon source glucose (albeit, both mutations caused a slight increase in lag phase) (**Fig. S8A**). Reduced growth rates can affect β-lactam sensitivity non-specifically [56] and mutants conferring slower growth can thus confound the interpretation of experiments conducted with such strains. Consistent with the expectation of reduced ETC activity in these mutants, disruption of *nqrA* and *ubiA* in both the WT and the Δ*vxrAB* mutant background resulted in a marked reduction in PenG-induced accumulation of H_2O_2, as measured by Amplex Red (**Fig. S8B**). To test the hypothesis that the reduction in H_2O_2 also results in lack of killing in the Δ*vxrAB* mutant, we conducted time-dependent killing experiments with these strains. As observed previously, WT viability remained stable for the entire duration of the experiment while the Δ*vxrAB* mutant displayed a ~10,000-fold decrease in viability. The Δ*nqrA* and *ubiA* mutants were as tolerant as the WT. However, a combination of ETC mutations with Δ*vxrAB* reproducibly increased survival by 10- (*nqrA*) or 100-fold (*ubiA*) (**Fig. 6A)**. Thus, maximal Δ*vxrAB* death after PenG exposure depends on the presence of the ETC.

ROS detoxification systems promote tolerance at high cell densities

We next asked whether ROS damage mitigation systems were required for WT tolerance. We created knockout mutants deficient in the iron starvation repressor Fur (expected to result in an increase in intracellular iron and thus enhanced ROS), SodB and a triple mutant defective in both catalases and OxyR1. We grew all strains from late exponential into stationary phase and periodically withdrew aliquots that were then

exposed to PenG for 3 h, and measured survival. As a comparison, we subjected the Δ*vxrAB* mutant to the same treatment. While all mutants except for Δ*vxrAB* exhibited wild-type survival patterns in exponential phase, entry into stationary phase coincided with significant killing in all mutants that are expected to experience enhanced ROS production (**Fig. 6B**). Consistent with these results, *sodB* had previously answered a Transposon Insertion Sequencing (TnSeq) screen for factors that are required for PenG tolerance [57]. We thus propose that ROS contribute significantly to β-lactam-mediated killing in stationary phase (see Discussion for details).

Penicillin exposure induces the Fur regulon

Thus far, we have shown that VxrAB controls iron acquisition and that a lack in the ability to do so may result in enhanced PenG-mediated killing. But why do PenG-treated Δ*vxrAB* cells increase their iron load? According to evidence presented above, H_2O_2 accumulates upon exposure to PenG. In *Bacillus subtilis,* peroxide is sensed by the transcriptional regulator PerR, a member of the Fur family of repressors [58]. PerR senses peroxide via oxidation of an iron cofactor [59], which results in induction of the PerR ROS detoxification regulon [60-62]. *V. cholerae*, like many other Gram-negative bacteria, lacks PerR; but in other bacteria, peroxide is thought to directly inactivate Fur through oxidation of its iron cofactor [63]. Derepression of the Fur regulon in turn would result in the upregulation of iron acquisition systems. To test the hypothesis that PenG induces the Fur regulon, we used S1 nuclease mapping to monitor transcript levels of the canonical Fur regulon readout *ryhB*[64], a small RNA [65]. Consistent with our line of thinking, *ryhB* was highly induced by addition of external H_2O_2 **(Fig. 7A).** In *E. coli, sodB*

transcript levels are negatively controlled by *ryhB,* and consistent with a similar regulatory mechanism in *V. cholerae, ryhB* induction (**Fig. 7A**) coincided with a disappearance of the *sodB* transcript during treatment with hydrogen peroxide (**Fig. 7A**). Consistent with a regulation via iron starvation sensing, *ryhB* transcript also increased dramatically upon exposure of cells to the cation chelator EDTA (**Fig. 7A**). Upon PenG exposure, *ryhB* transcript was reproducibly induced ~2-fold in both the WT and Δ*vxrAB* after 20 min, followed by a return to baseline. After prolonged PenG-treatment (180 min), *ryhB* remained uninduced in the WT, but increased dramatically in the Δ*vxrAB* mutant. Consistent with these transcriptional changes, a P_{ryhB}-*msfGFP* transcriptional reporter construct also increased in fluorescence after exposure to PenG in both, WT and Δ*vxrAB* (**Fig. 7B**). Other Fur-regulated genes (*hutA, hutB* and *vc2212*), also exhibited a marked, and in some cases transient, upregulation upon PenG exposure (**Fig. 7B**). These results suggest that indeed the Fur regulon is induced by exposure to PenG. Interestingly, we noticed in our ICP-MS dataset that concomitantly with iron uptake, manganese concentrations also increased in PenG-treated cells (**Fig. 7C**). Manganese has been proposed to be a cellular response to "rescue" iron-dependent enzymes that have lost their iron cofactor due to iron starvation or oxidative damage; biologically appropriate, Mn^{2+} uptake is thus under control of Fur in Gram-negative model organisms [66-68]. While a specific Mn^{2+} importer has not been identified in *V. cholerae* [69], our data suggest that the cholera pathogen might possess a similar regulatory arrangement.

Discussion

Our overall model of VxrAB-mediated tolerance is depicted in **Fig. 8;** based on the evidence presented in this study, we propose the following: PenG induces cell wall degradation, resulting in perturbations of the electron transport chain. Our work does not directly address the nature of this perturbation, but it may simply result from topological alterations of the cytoplasmic membrane brought about by loss of the cell wall. Interestingly, and consistent with this line of thinking, other cell wall deficient cells (L-Forms) also appear to accumulate ROS [70,71]. We hypothesize that partial reduction of molecular oxygen through the ETC (particularly NqrA) results in the production of superoxide O_2^-. O_2^- is removed by SOD, which catalyzes the formation of hydrogen peroxide (H_2O_2). H_2O_2 induces the *oxyR1* regulon, but we propose that it also inappropriately inactivates the Fur repressor via oxidation of its Fe^{2+} cofactor. Inactivation of Fur (i.e., induction of the Fur regulon) results in the upregulation of iron uptake systems, which increases the intracellular iron pool. Intracellular iron reacts with H_2O_2 to form hydroxyl radical $HO^{\cdot}$, which damages proteins and other macromolecules. The wild-type strain mounts effective responses to all these types of damage. SOD, AhpC and catalases detoxify superoxide and H_2O_2. VxrAB induces cell wall synthesis functions to prepare cells for speedy recovery once the antibiotic is removed. At the same time VxrAB also downregulates some iron acquisition genes and other Fur functions to dampen detrimental iron influx, and thus decrease oxidative damage. Interestingly, some of our data suggest that ROS production might contribute significantly to killing in later growth phases (early stationary phase), and stationary phase-specific oxidative damage is not without precedent. Periplasmic SODs are under

control of stationary phase regulators in diverse bacteria and yeast [72-74] and SOD is required for antibiotic tolerance in stationary phase in *P. aeruginosa* as well [75]. We hypothesize that during rapid growth in exponential phase, the primary mechanism of action (cell wall degradation) is likely the more important contributor to cell death, while in stationary phase (slower/no growth, less cell wall damage), the harmful effects of ROS accumulation may become more visible. This is noteworthy, since in the natural environment, bacterial growth can be expected to resemble stationary phase more than rapid growth in exponential phase [76]. On separate note, β-lactam-mediated killing in stationary phase may seem counterintuitive at first, since at least in the well-characterized model organism *E. coli*, cessation of growth upon entry into this growth phase is generally assumed to result in complete protection from β-lactam-induced damage [56,77]. However, the *vxrAB* mutant still exhibited significant PenG-dependent mortality even when PenG exposure only occurred several hours into stationary phase, i.e., far into a period of non-growth, suggesting that this mutant experiences PenG-induced cell envelope damage even when populations stop growing. We thus propose that in *V. cholerae,* cell wall turnover (and thus PenG's ability to inflict damage) continues at least for some time after cells stop growing. A similar phenomenon could explain the unusual observation that the Lyme disease pathogen *Borrelia burgdorferi* remains susceptible to killing by amoxicillin in stationary phase [78].

The connection between antibiotic exposure and ROS production and particularly the extent of the contribution of ROS to killing is still actively debated in the field. We agree with a previous hypothesis [34] that some of the interpretive difficulties in other studies

may have arisen from the low concentrations of antibiotics used (often around the MIC). High concentrations of bactericidal antibiotics might kill cells too quickly through their primary mechanism of action to measure a response to the proposed secondary mechanism. Lower concentrations around the MIC might result in day-to-day variation of killing dynamics that are difficult to reproduce under different conditions. In contrast, bacteria like *V. cholerae* (as well as *P. aeruginosa, Klebsiella pneumoniae, K. aerogenes* and *Enterobacter cloacae*), exhibiting almost population-wide tolerance to β-lactams [11,13,14,57], may be more appropriate model organisms to dissect the layers of physiological changes occurring as a consequence of antibiotic exposure. In these tolerant bacteria, the primary mechanism of action (degradation of the cell wall) is recapitulated; however, unlike in other bacteria, this does not result in lysis and cell death, allowing us to examine a large population of live cells after treatment with high concentrations (10 x MIC or more) of antibiotic.

One of the main critiques of the idea that ROS contribute to killing was that some groups failed to measure meaningful ROS levels (and the expected responses to them) in antibiotic-treated cells in the model organism *E. coli* [33,34]. This has been challenged by other groups [35,37,79]. Here, we have shown that *V. cholerae* accumulates ROS and induces defense systems against them after exposure to PenG. We propose that in the *vxrAB* mutant, antibiotic-induced lethality is multifactorial. Both, cell wall defects and ROS may contribute to killing. Importantly, other detrimental consequences of iron influx may also play a role, for example mismetalation of key enzymes [48]. While ROS production and iron influx are measurable in the wild type as well (to a lower degree

than the mutant), it is likely that its multiple, highly effective defense systems prevent antibiotic killing. This thinking is consistent with a previous observation that compared to *E. coli* and *P. aeruginosa,* exposure of *V. cholerae* to sub-MIC concentrations of β-lactam antibiotics only caused a moderate increase in mutagenesis (a possible consequence of ROS accumulation) [80]. Thus, the cholera pathogen's high tolerance to β-lactam exposure might be the consequence of an exceptional ability to repair cell damage.

Most means to directly probe the effect of ROS on cellular physiology under antibiotic stress are not without caveats. Growth under anaerobic conditions changes growth rates and thus response to antibiotics non-specifically (and it is for this reason that we did not consider killing under anaerobic conditions here). Bipyridyl might simply reduce metabolism in a subset of cells (those at the lower end of the iron content normal distribution), causing non-specific induction of "tolerance" through metabolic shutdown. While we cannot entirely rule out this possibility, we demonstrate that PenG-treatment simultaneously induces iron uptake and H_2O_2 production, raising the strong possibility that the increase in iron levels has toxic consequences. As a side-note, iron withdrawal is a common antibacterial strategy in the human host and might thus significantly affect antibiotic susceptibility *in vivo*, regardless of whether the mechanism is through metabolic shutdown or iron detoxification [81]. Since iron influx into antibiotic-stressed cells can also be detrimental, the extent of the host's ability to control iron levels in a specific infection locale might thus significantly and divergently influence antibiotic susceptibility in different host tissues.

While it is difficult to conclude beyond doubt that ROS contribute significantly to killing by antibiotics in the Δ*vxrAB* mutant and we thus hesitate to unequivocally do so here, we conclude that β-lactams (and likely other antibiotics) elicit more complex cellular responses than just those associated with their primary mechanism of action. A more context-, metabolism- and physiology-centered view of antibiotic action [82-85] might therefore yet yield critical insight to enable the development of novel adjuvants that increase the efficacy of antibiotics in the complex infection environment. Lastly, with or without ROS, our data suggest that targeting bacterial stress responses could be a powerful strategy to enhance the activity of bactericidal drugs against tolerant pathogens.

Acknowledgments

Research in the Dörr laboratory is supported by NIAID grant 1R01AI143704. This work was partially supported by the Korea Bio Grand Challenge Project (2018M3A9H3024759 to B.K.C.) through the National Research Foundation of Korea (NRF) funded by the Ministry of Science and ICT, Republic of Korea. We thank the Helmann lab (Cornell University) for sharing equipment and reagents. We further thank Stavroula Hatzios (Yale University), John Helmann (Cornell University), Joseph Peters (Cornell University), James Imlay (University of Illinois) and members of the Dörr lab for helpful comments.

Figure legends

Figure 1 | ChIP-Seq and RNA-Seq analysis reveals a complex VxrB regulon. (**A**) Overview of VxrB-binding profiles across the *V. cholerae* genome after β-lactam exposure (PenG 100µg/ml [10x MIC] for 3 hours). Red peaks indicate VxrB binding sites above the significance cutoff (q-value<10^{-10}; MACS). (**B**) RNA-Seq MA plot is presented as fold change between $VxrB^{D78E}$ overexpressed sample and control sample. Red dots indicate differentially expressed genes after $VxrB^{D78E}$ overexpression (P-value < 0.001). Representative VxrB target genes are marked on both chromosomes and on the MA plot. **(C)** Venn diagram depicting overlap between RNA-seq and ChIP-Seq datasets **(D)** Regulatory modes of representative VxrB-controlled genes in response to PenG. Upper plot shows VxrB binding patterns (assessed via ChIP-Seq), lower panel shows transcriptional response upon overexpression of $VxrB^{D78E}$ (assessed via RNA-Seq). RNA expression was confirmed by S1 nuclease mapping assay in wild type and *Δvxr*AB mutant strains after exposure to PenG (100 µg/ml for 3 hours).

Figure 2 | Peptidoglycan synthesis control only partially explains *Δvxr*AB lethality. **(A,B)** DNAse I footprinting results for VxrB interaction with promoters controlling cell wall synthesis functions. Red boxes indicate core DNA regions protected by purified VxrB protein (final concentration 0.17 - 1.38 µM) on the *murJ* (A) or *pbp1A* (B) promoter. Predicted start codons of each gene are presented in bold letters. VBS, putative **V**xrB **B**inding **S**equence **(C- E)** Reduction of cell wall synthesis gene expression causes a moderate tolerance defect. **(C)** Survival of a Δ*pbp1b* Δ*pbp1a* P_{iptg}:*pbp1a* strain after 6

hours of PenG exposure. P_{up} indicates conditions of high IPTG concentrations (100 µM), P_{down} low IPTG concentration (2 µM). Survival fraction is cfu/ml of PenG-treated cultures normalized to untreated cultures grown in and plated on medium containing the same IPTG concentration. **(D)** Deleting the putative VxrB binding site from the *murJ* promoter abrogates induction of *murJ* by PenG exposure. Transcript levels were measured by S1 nuclease mapping. Numbers represent induction as measured by band intensity, normalized to pre-exposure WT. n.d., not determined. (**E)** Time-dependent killing experiment in the presence of PenG (100 µg/ml, 10 x MIC). All data are means (+/- standard error) of 3 independent biological replicates.

Figure 3 | VxrAB controls genes involved in iron homeostasis. (A) Venn diagram showing overlap between the VxrB regulon and known *V. cholerae* Fur-controlled genes. (as per RegPrecise3.0 DB, http://regprecise.lbl.gov/RegPrecise/). 20 out of 47 Fur-regulated genes also have a VxrB binding site and are differentially regulated by $VxrB^{D78E}$. (**B)** Genomic organization of iron uptake systems and their putative Fur/VxrB binding sites. **(C)** Time-course of iron accumulation in PenG-treated WT and Δ*vxrAB* cells as measured by ICP-MS. Data are average of 3 independent biological replicates, error bars represent standard deviation. ∗∗P=0.001; ∗∗∗P<0.0003 (paired t-test) **(D)** Streptonigrin-sensitivity of PenG-treated cells. Cultures were grown to a density of ~2 x 10^8 cfu/ml. Before ("- PenG") and after addition of PenG (100 µg/ml, 10x MIC), ~ 5 x 10^7 cells were spread on an LB agar plate. In the PenG-treated samples ("+ PenG"), beta lactamase solution was also added to remove the antibiotic. Streptonigrin (5 mg/ml, in DMSO) was then added on a filter disk, followed by incubation for 24 h at 37 ˚C. Values

represent average diameter of clearance zones (+/- standard deviation) of six biological replicates. SNG, streptonigrin. **(E)** Iron chelation reduces Δ*vxrAB* death in the presence of PenG. Time-dependent killing experiment in the absence or presence of 250 μM bipyridyl (Bip) with or without addition of 250 μM Fe^{2+}. Data are average of 3 independent biological replicates, error bars represent standard deviation.

Figure 4 | PenG exposure induces ROS defense systems (A) RNA expression profiles of first line ROS defense systems in *V.cholerae* monitored by S1 mapping assay. Wild type and *Δvxr*AB were grown to exponential phase (OD_{600}~0.5) in liquid LB medium and treated with 100ug/ml PenG. Samples were collected at different time points as indicated and S1 nuclease protection assay carried out to quantify the expression level of each gene. Quantified average values (normalized to WT before PenG exposure) from three independent experiments are presented under the signals of each gene. **(B)** Gel based catalase and superoxide dismutase (SOD) activity staining. Wild type and *Δvxr*AB cells were grown to exponential phase (OD_{600}~0.5) in LB medium and exposed to PenG. Samples were collected at the indicated time points. 30 μg/well of crude proteins were separated by 5% (catalases) or 8% (SODs) native PAGE at 4 °C followed by staining (see Methods for details). To quantify the SOD or catalases activity, stained gels were scanned and analyzed by Odyssey Imaging Systems (LI-COR Biosciences) and Image Studio Lite software. Rpol α subunit (RNA polymerase I, α subunit) was visualized as internal control. Coomassie staining (loading control) was used to ensure consistent protein loading between samples. **(C)** and **(D)** Quantified activity values from the gel shown in **(B)**. Data are average values from three

independent experiments normalized to untreated wild type, for **(C)** catalase or **(D)** superoxide dismutase activity.

Figure 5 | PenG induces hydrogen peroxide production and protein oxidation (A) **(A-B)** Total intracellular **(A)** or supernatant **(B)** hydrogen peroxide (H_2O_2) levels were measured using Amplex^{TM} Red Hydrogen Peroxide/Peroxidase Assay Kit and normalized to total cellular protein level (measured by Qubit^{TM}). Data are average values from three independent experiments, error bars represent standard deviation. Insert represents magnified data to accentuate subtle differences between mutants and conditions. Cat, catalase. **(C)** Detection of proteins damage following oxidative stress triggered by PenG treatment. To measure the total cellular protein oxidation, OxyBlot Protein Oxidation Detection Kit (Sigma-Aldrich) was used. Wild type and *Δvxr*AB mutant were grown to OD_{600}~0.4 and harvested at different times after PenG treatment. 0.5 mM H_2O_2 treated cells were used as a positive protein oxidation control with oxidized standard marker ($_{OX}$M). Both DNP-derivatized or nonderivatized (negative control) protein samples were separated by polyacrylamide gel electrophoresis followed by Western blotting with-DNP specific antibody.

Figure 6 | ROS generation and detoxification modulate PenG-induced lethality

(A) Time-dependent killing of respiratory chain mutants (Δ*nqrA,* encoding NADH dehydrogenase and Δ*ubiA*, encoding an early step of ubiquinone synthesis) in the presence of PenG (100 µg/ml, 10xMIC). All strains were grown in LB 0.2 % glucose. Data are mean of three independent biological replicates, error bars represent standard

deviation. **(B)** Growth-phase dependent killing assay. At designated time-points, a 5 ml aliquot was withdrawn and exposed to 100 µg/ml PenG for 3 h. Cfu/ml for each time point was assessed before (solid lines) and after addition of PenG (dotted lines).

Figure 7 | PenG and hydrogen peroxide induce the Fur iron starvation response. **(A)** Expression levels of the Fur-regulated small RNA *ryhB* and the RyhB target *sodB* were quantified using S1 nuclease mapping. Cells were grown to mid-exponential phase followed by exposure to H_2O_2, PenG or the positive control 2 mM EDTA (a strong chelator of divalent cations) for the indicated duration. Numbers represent expression levels normalized to untreated control (averages from three independent replicates). **(B)** To confirm the induction of *ryhB* transcript by PenG treatment, the native *ryhB* promoter was fused with *msfGFP* and introduced into WT and *ΔvxrA* mutant cells. Each strain was cultured until mid-exponential phase, when 1mM EDTA, 0.5mM FeCl or 100µg/ml PenG were added for the indicated duration. PenG-mediated induction of other Fur-regulated genes (*hutA/B*, coding for heme transport systems and *vc2212*, which encodes a component of a ferric citrate uptake system) was measured by S1 nuclease mapping. **(C)** Time-course of manganese accumulation in PenG-treated WT and Δ*vxrAB* cells as measured by ICP-MS. Data are average of 3 independent biological replicates, error bars represent standard deviation. $^{**}P=0.001$; $^{***}P<0.0003$ (paired t-test)

Figure 8 | Proposed model for VxrAB-mediated antibiotic tolerance.

PenG induces ETC dysfunction, resulting in the production of ROS. Hydrogen peroxide illegitimately induces the Fur regulon, resulting in the upregulation of iron acquisition systems, resulting in enhanced iron influx and oxygen radical generation. VxrAB dampens this response by downregulating iron acquisition genes, in addition to its primary role as a positive regulator of cell wall synthesis genes. SO, superoxide.

MATERIALS AND METHODS

Bacterial strains and culture conditions.

All *V. cholerae* strains used in this study were derivatives of *V. cholerae* WT El Tor strain N16961 (Heidelberg *et al.,* 2000) or E7946 (for chitin-induced transformation) listed in Table S1. *V. cholerae* was grown on Luria-Bertani (LB) medium with or without 0.2% glucose or in M9 medium containing 0.2% glucose at 37°C unless otherwise indicated. All media contained 200 µg/ml streptomycin (to which *V. cholerae* is resistant). Where applicable, growth media were supplemented with 100 µg/ml Benzylpenicillin potassium salt (PenG) (Fisher BioReagents, cat# BP914-100), isopropyl-β-D-1-thiogalactopyranoside (IPTG; final 0.1~1mM) (GOLDBIO, cat# 12481C50), or catalase 1µg/ml (Sigma-Aldrich, Cat# c9322)**.** *Escherichia coli* DH5α and DH5α λpir were used for routine DNA cloning (Sambrook *et al*., 1989 and Platt R *et al.,* 2000). Unless indicated otherwise, LB liquid media were inoculated from an overnight culture and incubated at 37°C with shaking at 200 rpm until reaching mid-exponential phase (OD_{600} ~0.4). Where applicable, trimethoprim (Sigma, cat #T7883, dissolved in DMSO) was used at 15 µg/ml final concentration.

Strain construction

Deletion mutants were generated via replacement of the open reading frame/binding site with the scar sequence TAATGCGGCCGCACTCGAGTAATAATGATGA or, where indicated, a trimethoprim resistance cassette. Knockouts were generated either by homologous recombination using the suicide vector pCVD442 [86] or by chitin-induced

natural transformation, both as described before [87] [17]. The following primer combinations were used (see supplemental material for sequence information).

murJ Δvbs: TDP1062/1064 + TDP1066/1067, fused via stitching PCR with nesting primers TDP1078/1079, followed by chitin transformation using *vc1807*::trim (generated using primers TDP597/598 + TDP599/600 [on trimR from the V. cholerae HAITI strain [88]] +TDP601/602, fused via stitching PCR with nesting primers TDP603/604) as primary selection.

Δ*oxyR1*: TDP1057/58 + TDP1059/60, cloned into Xba1-digested pCVD442 using isothermal assembly [89], followed by knockout via homologous recombination.

Δ*katG:* TDP1100/1101 + TDP1102/1103, cloned into Xba1-digested pCVD442 using isothermal assembly, followed by knockout via homologous recombination.

Δ*katB*: TDP1103/1104 + TDP1105/1106, cloned into Xba1-digested pCVD442 using isothermal assembly, followed by knockout via homologous recombination.

lacZ::P_{ryhB}:*msfGFP*: TDP1152/1235 + TDP1237/38, cloned into Sma1-digested pTD101, a suicide vector for chromosomal integration into the *lacZ* locus [90].

Δ*nqrA*: TDP1388/1389 + TDP1390/1391, fused via stitching PCR with nesting primers TDP1392/1393, followed by chitin transformation using *vc1807*::trim (see above) as primary selection.

Δ*ubiA*::*trim* TDP1399/1401 + TDP1404/1403 + TDP636/637, fused via stitching PCR with nesting primers TDP1405/1406, followed by chitin transformation.

Δ*sodB*: TDP828/829 + TDP830/831, cloned into Xba1-digested pCVD442 using isothermal assembly, followed by knockout via homologous recombination.

Δ*fur*: TDP834/835 + TDP836/837, cloned into Xba1-digested pCVD442 using isothermal assembly, followed by knockout via homologous recombination.

Pulldown of VxrB binding DNA fragments and ChIP-Seq library construction. Cells carrying either 6xHis+VxrB or the native gene were grown in LB medium to mid-logarithmic phase (at an OD_{600} ~0.5). Following treatment with PenG (100 µg/ml, 3 hours), 30 ml aliquots were spun down and the pellets were saved at -80°C. For cross-linking, pellets were resuspended in 1ml buffer CJ1 [100 mM Na_2HPO_4, 600 mM NaCl, and 5 mM imidazole;pH 8.0] and 30 µl of 34% formaldehyde was added, followed by rocking at room temperature for 10 min. To quench cross-linking reaction, 133 µl of 1 M Glycine pH7.5 (final molar concentration 0.133 M) was added, and the cells were shaken gently at 4°C for 30 min. Cells were collected by centrifugation, and the pellets were resuspended in 1 ml buffer CJ2 [100 mM Na_2HPO_4, 600 mM NaCl, 0.05% tween™, and 30 mM imidazole;pH 8.0] after washing twice with same CJ1 buffer. Cells were then lysed by sonication, followed by addition of Micrococcal nuclease (100 U ml^{-1}, NEB cat# M0247S) and RNase A (1 mg ml^{-1}) for fragmentation of genomic DNA and removal of RNA. 950 µl of supernatant was collected after centrifugation.

For DNA-VxrB complex purification, HisPur™ Ni-NTA magnetic beads (cat#88831-Thermo Scientific) were equilibrated with six bed volumes of CJ2 buffer [100 mM Na_2HPO_4, 600 mM NaCl, 0.05% tween™, and 30 mM imidazole;pH 8.0]. 500 µg of crude lysate (protein concentration determined by Bradford assay) was mixed with the Ni-NTA resin and incubated at 4°C for 4 hours on rotation mixer. The bead slurry was recovered via magnetic stand for 5 min standing and washed twice with 400 µl buffer

CJ3 [100 mM Na_2HPO_4, 600 mM NaCl, 0.05% tween^{TM}, and 50 mM imidazole; pH 8.0]. The VxrB-DNA complexes were then eluted from the beads by addition of CJ4 elution buffer [100 mM Na_2HPO_4, 600 mM NaCl, 0.05% tween^{TM}, and 500 mM imidazole;pH 8.0]. Enriched target DNAs were purified by using PCR Clean-Up Kits (Thermo Fisher Scientific) after reversal of crosslinking at 65°C overnight. The desired DNA fragment size (200~300 bps) was then purified by gel extraction. For illumina HiSeq, each DNA library was constructed with specific barcode sequences, according to the manufacturer's instruction of TruSeq ChIP Library Preparation Kit (IP-202-1012, Illumina). The constructed libraries were sequenced using 100-bp paired-end read protocol on an Illumina HiSeq 2500 platform (Illumina) at the Biotechnology Resource Center (BRC) at Cornell University.

ChIP-Seq, binding peak detection, and motif analysis. Sequencing data was processed by CLC Genomics Workbench (CLC Bio). First, raw sequencing reads were quality trimmed using a Trim Sequence Tool with a quality limit of 0.05. Any reads with more than two ambiguous bases were discarded at this step. Then, quality trimmed reads were mapped onto the *V. cholerae* reference genome (NCBI accession NC_002505.1 and NC_002506.1) with mismatch cost of 2, insertion/deletion cost of 3, length fraction of 0.9, and similarity fraction of 0.9. Non-specific matches were mapped randomly. Mapping files (.bam) were submitted to the Model-based Analysis of ChIP-Seq 2 (MACS2) software with a mapping file of a mock sample as a control (Zhang *et al*., 2008). Peaks were detected with shift size of 50 and q-value cutoff of 10^{-10}. For motif analysis, peaks with q-value lower than 10^{-40} were selected and 100 bp DNA sequences

centered at peak summits were submitted to MEME Suite software v4.11.4 (Bailey *et al*., 2009).

RNA-Seq analysis

Sequencing data (obtained previously) were also processed on a CLC Genomics Workbench (CLC Bio). Raw sequencing reads were quality trimmed with the same method with ChIP-Seq reads. Quality trimmed reads were mapped strand specifically on the reference genome sequence by Transcriptome Analysis Tool with the following parameters: maximum number of mismatches of 2, length fraction, and similarity fraction of both 0.9. Number of mapped reads on each gene was normalized by DESeq2 package in Bioconductor v3.4 (Love *et al*., 2014). Genes with p-value (padj, DESeq2) lower than 0.001 were scored as differentially expressed genes (DEGs).

Purification of VxrB protein. Wild-type VxrB protein was purified from *E. coli* BL21 (DE3/pLysS) cells containing pET15b based recombinant plasmid. The coding sequence for WT VxrB was cloned into pET15b (Novagen) into the *Nde*I and *Bam*HI restriction sites. For purification of VxrB from this construct, an overnight culture from a single colony was used to inoculate 1 liter of LB medium. Cells were grown with vigorous shaking at 37°C to an optical density at 600 nm (OD_{600}) of 0.5 and were induced with 1 mM (final concentration) isopropyl-β-D-thiogalactopyranoside (IPTG) for 6 h at 30°C. Harvested cells were re-suspended in binding buffer [20 mM Tris-HCl (pH 7.9), 0.5 M NaCl, 1 mM TCEP (tris(2-carboxyethyl)-phosphine), and 5 mM imidazole] and cell extracts were prepared by sonication and centrifugation at 16,000 rpm for 45

min. Cell extracts were loaded onto a cobalt-charged NTA column and then washed with 6 volumes of binding buffer followed by 6 volumes of washing buffer [20 mM Tris-HCl (pH 8.0), 0.5 M NaCl, and 50 mM imidazole]. VxrB protein was eluted with 10 volumes of elution buffer [20 mM Tris-HCl (8.0) and 0.5 M NaCl] containing linear imidazole gradients from 100 to 500 mM. Fractions containing VxrB protein were pooled and dialyzed against buffer J1 [20 mM Tris-HCl (pH 8.0), 250 mM NaCl, 5% (vol/vol) glycerol, and 4 mM EDTA] to remove imidazole and cobalt and then transferred to two extra dialysis buffer J2 [20 mM Tris-HCl (pH 8.0), 150 mM NaCl, 10% glycerol, and 0.2 mM DTT] and buffer J3 [20 mM Tris-HCl (pH 8.0), 150 mM NaCl, 30% glycerol, and 1 mM DTT]. The purified VxrB protein was concentrated by centrifugal filter devices (Millipore, 3,000 MW CO) before injection onto High load TM (16/60) pg Superdex G75 column in FPLC system (Pharmacia). The column was equilibrated with buffer SG [20 mM Tris-HCl (pH 8.0), 150 mM NaCl, and 1 mM DTT]. Eluted fractions were monitored through UV detector. Concentration of purified VxrB was estimated in triplicate by Bradford assay (Bio-Rad) using BSA (bovine serum albumin, Sigma-Aldrich) as the calibration standard at A595. Measurement of UV absorbance at 280 nm, combined with calculated molar extinction coefficient (ε_{280} = 46470 M^{-1} cm^{-1}, http://expasy.org/cgi-bin/protparam), gave nearly identical values. The purity of protein was confirmed through Coomassie blue staining of loaded protein samples in the SDS-PAGE gel. The protein was stored in final storage buffer JHS [20 mM Tris-HCl (pH 8.0), 150 mM NaCl, 1 mM DTT, 30% Glycerol, 1 mM $MgCl_2$, and 1 mM ATP] at -80°C.

DNase I footprinting assay. The probe DNAs were prepared by using the "crush and soaking method" (Sambrook *et al*., 1989) after PCR with the primer pairs shown in Table S2. The 5′ end of the probes was labeled with 6-FAM (Fluorescein). Binding reactions were performed as described below for EMSA, except using 250 ng probe DNA in a 40 µl reaction mixture. DNA probes were incubated with increasing concentrations of VxrB (0.17, 0.34, 0.68, and 1.38 µM). After 20 min incubation at room temperature, 40 µl of 5 mM $CaCl_2$ and 10 mM $MgCl_2$ was added, followed by adding 200 U of RQI RNase-free DNase I (Promega) for 1 min. The cleavage reaction was stopped by adding 90 µl stop solution (200 mM NaCl, 30 mM EDTA, 1% sodium dodecyl sulfate, 125 µg ml^{-1} of glycogen), followed by DNA extraction and precipitation. Samples were analyzed by capillary electrophoresis on an ABI 3730x1 DNA analyzer (Life Technologies). The DNA probe only with no added VxrB was analyzed in parallel. The core protected regions were indicated with red lines and its corresponding DNA sequences were shown at the bottom of peak profiles.

Preparation of total RNA and S1 nuclease mapping analysis. Wild type and mutant strains were cultured to mid-logarithmic phase (at an OD_{600} of 0.4 to 0. 5) in LB medium. Following application of a stress (PenG or H_20_2), total RNA was extracted using the "hot phenol method" as described in Shin *et al*., 2014, albeit without lysozyme pretreatment. RNA was quantified and quality-controlled by absorbance spectroscopy and confirmed by resolving RNA samples on 1.3% formaldehyde-agarose gels. Gene-specific DNA oligonucleotide probes for *vxrA*, *vxrB*, *pbp1A*, *zapB*, *flaA*, *murJ*, *oxyR1*, *sodB*, *sodA*, *katG*, *katB*, *prxA*, *oxyR2*, *ahpC*, *dps*, *fur*, and *ryhB* transcripts were

generated by PCR amplification using *V. cholerae* wild-type genomic DNA as template. The appropriate primer pairs are listed in Table S2. Each specific DNA probe was radiolabeled with (γ-^{32}P) ATP and T4 polynucleotide kinase and 30,000-40,000 cpm of labeled probe was used in each reaction. For S1 assays, 100 µg of total RNA was pelleted and lyophilized. The total RNA pellet was then carefully resuspended in 20 µl hybridization buffer [40 mM PIPES (pH 6.4), 400 mM NaCl, 1 mM EDTA, 80% (v/v) formamide]. Individual samples were incubated at 95°C for 25 min and cooled to 42°C. Following overnight incubation, 300 µl of S1 nuclease mix containing 100 units of S1 nuclease in S1 nuclease buffer [280 mM NaCl, 30 mM NaOAc (pH 4.4), 4.5 mM ZnOAc] was added and incubated at 37°C for 45 min. The reaction was terminated by addition of 75 µl of S1 nuclease termination solution (2.5 M NH_4OAc, 0.05 M EDTA). The DNA-RNA hybrid was precipitated by adding 400 µl of isopropanol (100 % v/v) and the pellet was washed with 70% (v/v) ethanol, vacuum dried, and re-suspended in 13 µl alkaline loading dye (Sambrook *et al*., 1989). The protected DNA fragments were then resolved by 6% (w/v) polyacrylamide gels containing 7 M urea. Gels were dried using a Hoefer Scientific Drygel Slab Gel Dryer 01385 and then imaged on a phosphor imaging screen (Typhoon FLA 7000; GE); bands were quantified using Multi Gauge V3.0 (Fuji). Quantified average fold intensity (compared to non-treated sample) from three independent experiments were presented under the each signal with standard deviation values.

Killing Assay. For most time-dependent killing experiments, overnight cultures of wild type and each mutant strains were grown at 37°C in LB medium in the presence or

absence of additional supplement such as IPTG or 0.2% glucose. At each time-point, samples were collected, serially diluted (sterile PBS) and spot-plated for cfu/ml determination (plates were incubated at 30 ˚C for 20 – 24 h). Where indicated, PenG (100 µg/ml), 250 µM Bip, or 250 µM $FeCl_2$ were added. For the growth phase dependent experiment, wild type, *ΔvxrAB*, *Δfur*, *ΔsodB* and *ΔoxyR1ΔkatGΔkatB* mutants were cultured in the presence of 1µg/ml catalase for overnight seed (catalase is required for ΔoxyR1 growth) in 100 mL LB in flasks. At designated time points, 5ml cell cultures were transferred to new tubes and cultured with or without PenG for 3 hours; cfu/mL was determined before and after addition of the antibiotic.

Streptonigrin sensitivity assay

Cells were diluted 100fold from overnight cultures and grown to a density of ~2 x 10^8 cfu/ml. At each time point (before addition of 100 µg/ml PenG and 3 h after), 200 µL of culture were spread on 25 ml LB agar plates using glass beads. At the 3 h time point, 1 mg/ml (final concentration) β-lactamase (Sigma, catalog # P4524) was added prior to plating. Following plating, a sterile filter disk containing 5 µL of 5 mg/ml streptonigrin solution (Sigma, catalog # S1014, dissolved in DMSO) was placed in the center of the plate. Plates were then incubated 24 h at 37 ˚C. Measurements are averages of six biological replicates.

ICP-MS analysis for intracellular metal concentration measurement. A single colony of the indicated *V. cholerae* strains from LB plates was inoculated into 5 mL LB with streptomycin (200 µg/mL) and grown overnight. The next morning, 0.1% of

832 overnight cultured seeds were inoculated in 200 ml LB supplemented with antibiotics.
833 These cells were grown shaking at 37°C for 2~3 hours until they reached an OD_{600} of
834 ~0.5. Samples were collected before and at indicated time points after PenG treatment.
835 At the indicated time points, cells were pelleted by centrifugation (10 min, 20000 rcf)
836 and washed three times with phosphate buffered saline (PBS) buffer containing 0.1 M
837 EDTA followed by two chelex (BioRad, cat # 1422822)-treated PBS buffer washes to
838 remove all external metal ions. Cells were then resuspended in 400 µl of chelex-treated
839 PBS buffer with 1% Triton X-100 containing 75 mM NaN3 to induce lysis (Jolliffe et al.,
840 1981) and incubated at 37°C for 90 min. 10 µl of each supernatant was used to
841 measure total cell protein concentration by Bradford assay. 600 µl of 5% HNO3 with 0.1%
842 (v/v) Triton X-100 were then added to the rest of the supernatant, which was boiled at
843 95°C for 30 min. After centrifugation (10 min, 20000 rcf), the supernatant was then
844 diluted 1000fold with 1% HNO3. Metal levels were measured by ICP-MS (Perkin-Elmer
845 ELAN DRC II using ammonia as the reaction gas and gallium as an internal standard)
846 and normalized against total cell protein concentration. Data represent with average
847 values from biological triplicates. Significant differences between wild type and *Δvxr*AB
848 after PenG exposure were determined by paired R t-test as indicated: ∗∗P=0.001;
849 ∗∗∗P<0.0003.
850
851 **Catalase and SOD activity assay.** Catalase activity staining was performed as
852 described in Cho *et al.,* 1997. Briefly, cell extracts (30 µg per well, obtained by 20 cycles
853 of sonication on ice at 20 % power, 3 s pulse, followed by 10 s cooling) were separated
854 on a 5% native polyacrylamide gel and electrophoresed at 4°C with 80 volt. The gel was

washed in distilled water and then treated with 1 mM H_2O_2 for 20 min. After treatment, the gel was rinsed and transferred to 1% (w/v) ferric chloride and 1% (w/v) potassium ferricyanide solution. The reaction was stopped by washing twice in distilled water. Superoxide dismutase activity staining was performed as described in [91]. The cell extracts (30 µg/well) were electrophoresed on a 8% native polyacrylamide gel under the same conditions as described above for catalase activity, after which the gel was incubated in a solution containing 2.5 mM nitroblue tetrazolium (NBT) for 25 min and then in 50 mM phosphate buffer (pH 7.8) containing 28 µM riboflavin and 28 mM tetramethyl ethylene diamine for 20 min in the dark. The gel was placed in distilled water and exposed on a light box for 15 min until the dark blue background color appeared. To quantify SOD and catalase activity, stained gels were scanned and analyzed by Odyssey Imaging Systems (LI-COR Biosciences) and Image Studio Lite software. Quantified average values from three independent experiments are presented as a fold activity against wild type non-treated sample for SODs and Catalases.

Western blot analysis to detect alpha subunit of RNA polymerase. For the internal control of SOD and catalase activity, the same crude extracts were resolved on two independent 12 % polyacrylamide gels for each western blotting and coomassie staining. After electrophoresis the proteins were transferred to a membrane by using a semi-drying transfer system (I Blot 2-Invitrogen). The membrane was then blocked with blocking solution (dry skim milk dissolved in 20 mM Tris-HCl (pH7.8), 150 mM NaCl, 0.1% Triton X-100) overnight. The membrane was incubated with monoclonal anti-αRpol antibody (BioLegend-cat#663104) for two hours, washed with TBST (20 mM

878 Tris-HCl (pH7.8), 150 mM NaCl, 0.1% Triton X-100), and incubated with anti-mouse
879 secondary antibody (IRDye 800CW, Li-Cor cat# 926-32211). All images were scanned
880 on an Odyssey CLx imaging device (LI-COR Biosciences) and visualized using image
881 studio lite software.
882
883 **Measurement of total cellular H_2O_2 level.** Total cellular hydrogen peroxide (H_2O_2)
884 level was measured using the Amplex™ Red Hydrogen Peroxide/Peroxidase Assay Kit
885 (Invitrogen™ cat#A22188) and normalized to total cellular proteins. Wild type and
886 indicated mutant stains were cultured in LB medium (in the absence or presence of
887 additional 0.2% glucose when it needed) until OD_{600} ~0.5. PenG (100 µg/ml) was then
888 added and 1ml cell culture was withdrawn and pelleted at each indicated time point.
889 Pellets were resuspended in 100 µl cold 1xPBS buffer and lysed by sonication, followed
890 by centrifugation at 4°C (10 min, 20000 rcf). 3 µl of each supernatant was used to
891 measure total cell protein concentration by Bradford assay. 20µl extracts from cleaned
892 supernatant were reacted with kit components following manufacturer's instruction. For
893 H_2O_2 quantification, the reaction product resorufin was read by fluorometer (QUBIT 3,
894 Invitrogen) at Ex/Em of: ~571/585 nm. Obtained values were normalized to total protein
895 concentration.
896
897 **Detection of oxidized proteins.** Oxidized proteins containing carbonyl groups were
898 detected using the OxyBlot Protein Oxidation Detection Kit (Sigma-Aldrich: cat#S7150).
899 Briefly, wild type and *Δvxr*AB mutant were grown to exponential growth phase and
900 harvested at different times after PenG treatment. 0.5 mM H_2O_2 treated cells were used

as a positive protein oxidation control with oxidized standard marker ($_{OX}$M). The protein sample (10µg/well) was incubated with dinitrophenylhydrazine (DNPH) (derivatization reaction) for 15 min, followed by neutralization with a solution containing glycerol and β-mercaptoethanol. Both DNP-derivatized or nonderivatized (for negative control) protein samples were electrophoresed on a 10% SDS-PAGE and then transferred to a nitrocellulose membrane. After blocking, the membrane was incubated for 1 h with a rabbit antibody against DNP (cat# D9656), followed by incubation with secondary antibody: goat anti-rabbit IgG (Li-COR, IRDye® 800CW cat# 926-32211) for 1 h at room temperature as recommended by the manufacturer. The signals were scanned on an Odyssey CLx imaging device (LI-COR Biosciences) and visualized using image studio lite software.

Microscopy. All images were taken on a Leica MDi8 microscope (Leica Microsystems, GmbH, Wetzlar, Germany) with a PECON Temp-Controller 2000-1 (Erbach, Germany), heated stage at 37 °C for growth experiments, or room temperature. Time-lapse microscopy was performed by imaging frames five minutes apart and data were analyzed by ImageJ program. The msfGFP expressing cells were imaged at $485_{Ex}/530_{Em}$ for two second exposure time. Collected images were processed in ImageJ by subtracting background and adjusting brightness/contrast uniformly across all fluorescent images. Representative images were taken at least three independent experiments.

1. Spellberg, B. The future of antibiotics. *Crit Care* **18**, 228 (2014).
2. Fair, R.J. & Tor, Y. Antibiotics and bacterial resistance in the 21st century. *Perspect Medicin Chem* **6**, 25-64 (2014).
3. Lewis, K. Persister cells: molecular mechanisms related to antibiotic tolerance. *Handb Exp Pharmacol*, 121-133 (2012).
4. Lewis, K. Persister cells. *Annu Rev Microbiol* **64**, 357-372 (2010).
5. Lewis, K. Persister cells, dormancy and infectious disease. *Nat Rev Microbiol* **5**, 48-56 (2007).
6. El-Halfawy, O.M. & Valvano, M.A. Antimicrobial heteroresistance: an emerging field in need of clarity. *Clin Microbiol Rev* **28**, 191-207 (2015).
7. Wilmaerts, D., Windels, E.M., Verstraeten, N. & Michiels, J. General Mechanisms Leading to Persister Formation and Awakening. *Trends Genet* **35**, 401-411 (2019).
8. Balaban, N.Q.*, et al.* Definitions and guidelines for research on antibiotic persistence. *Nat Rev Microbiol* (2019).
9. Kitano, K., Tuomanen, E. & Tomasz, A. Transglycosylase and endopeptidase participate in the degradation of murein during autolysis of Escherichia coli. *J Bacteriol* **167**, 759-765 (1986).
10. Flores-Kim, J., Dobihal, G.S., Fenton, A., Rudner, D.Z. & Bernhardt, T.G. A switch in surface polymer biogenesis triggers growth-phase-dependent and antibiotic-induced bacteriolysis. *Elife* **8**(2019).
11. Dorr, T., Davis, B.M. & Waldor, M.K. Endopeptidase-mediated beta lactam tolerance. *PLoS Pathog* **11**, e1004850 (2015).
12. Cho, H., Uehara, T. & Bernhardt, T.G. Beta-lactam antibiotics induce a lethal malfunctioning of the bacterial cell wall synthesis machinery. *Cell* **159**, 1300-1311 (2014).
13. Monahan, L.G.*, et al.* Rapid conversion of Pseudomonas aeruginosa to a spherical cell morphotype facilitates tolerance to carbapenems and penicillins but increases susceptibility to antimicrobial peptides. *Antimicrob Agents Chemother* **58**, 1956-1962 (2014).
14. Cross, T.*, et al.* Spheroplast-mediated carbapenem tolerance in Gram-negative pathogens *Antimicrob Agents Chemother* (2019).
15. Errington, J., Mickiewicz, K., Kawai, Y. & Wu, L.J. L-form bacteria, chronic diseases and the origins of life. *Philos Trans R Soc Lond B Biol Sci* **371**(2016).
16. Errington, J. Cell wall-deficient, L-form bacteria in the 21st century: a personal perspective. *Biochem Soc Trans* **45**, 287-295 (2017).
17. Dorr, T.*, et al.* A cell wall damage response mediated by a sensor kinase/response regulator pair enables beta-lactam tolerance. *Proc Natl Acad Sci U S A* **113**, 404-409 (2016).
18. Dörr, T., Lewis, K. & Vulic, M. SOS response induces persistence to fluoroquinolones in Escherichia coli. *PLoS Genet* **5**, e1000760 (2009).

19. Raivio, T.L. Everything old is new again: an update on current research on the Cpx envelope stress response. *Biochim Biophys Acta* **1843**, 1529-1541 (2014).
20. Helmann, J.D. Bacillus subtilis extracytoplasmic function (ECF) sigma factors and defense of the cell envelope. *Curr Opin Microbiol* **30**, 122-132 (2016).
21. Radeck, J., Fritz, G. & Mascher, T. The cell envelope stress response of Bacillus subtilis: from static signaling devices to dynamic regulatory network. *Curr Genet* **63**, 79-90 (2017).
22. Wall, E., Majdalani, N. & Gottesman, S. The Complex Rcs Regulatory Cascade. *Annu Rev Microbiol* **72**, 111-139 (2018).
23. Guest, R.L. & Raivio, T.L. Role of the Gram-Negative Envelope Stress Response in the Presence of Antimicrobial Agents. *Trends Microbiol* **24**, 377-390 (2016).
24. Bhagirath, A.Y.*, et al.* Two Component Regulatory Systems and Antibiotic Resistance in Gram-Negative Pathogens. *Int J Mol Sci* **20**(2019).
25. Bury-Mone, S.*, et al.* Global analysis of extracytoplasmic stress signaling in Escherichia coli. *PLoS Genet* **5**, e1000651 (2009).
26. Cheng, A.T., Ottemann, K.M. & Yildiz, F.H. Vibrio cholerae Response Regulator VxrB Controls Colonization and Regulates the Type VI Secretion System. *PLoS Pathog* **11**, e1004933 (2015).
27. Teschler, J.K., Cheng, A.T. & Yildiz, F.H. The Two-Component Signal Transduction System VxrAB Positively Regulates Vibrio cholerae Biofilm Formation. *J Bacteriol* **199**(2017).
28. Dwyer, D.J., Kohanski, M.A., Hayete, B. & Collins, J.J. Gyrase inhibitors induce an oxidative damage cellular death pathway in Escherichia coli. *Mol Syst Biol* **3**, 91 (2007).
29. Kohanski, M.A., Dwyer, D.J., Hayete, B., Lawrence, C.A. & Collins, J.J. A common mechanism of cellular death induced by bactericidal antibiotics. *Cell* **130**, 797-810 (2007).
30. Kohanski, M.A., Dwyer, D.J., Wierzbowski, J., Cottarel, G. & Collins, J.J. Mistranslation of membrane proteins and two-component system activation trigger antibiotic-mediated cell death. *Cell* **135**, 679-690 (2008).
31. Dwyer, D.J., Kohanski, M.A. & Collins, J.J. Role of reactive oxygen species in antibiotic action and resistance. *Curr Opin Microbiol* **12**, 482-489 (2009).
32. Imlay, J.A. Diagnosing oxidative stress in bacteria: not as easy as you might think. *Curr Opin Microbiol* **24**, 124-131 (2015).
33. Liu, Y. & Imlay, J.A. Cell death from antibiotics without the involvement of reactive oxygen species. *Science* **339**, 1210-1213 (2013).
34. Keren, I., Wu, Y., Inocencio, J., Mulcahy, L.R. & Lewis, K. Killing by bactericidal antibiotics does not depend on reactive oxygen species. *Science* **339**, 1213-1216 (2013).
35. Hong, Y., Zeng, J., Wang, X., Drlica, K. & Zhao, X. Post-stress bacterial cell death mediated by reactive oxygen species. *Proc Natl Acad Sci U S A* **116**, 10064-10071 (2019).
36. Dwyer, D.J., Collins, J.J. & Walker, G.C. Unraveling the physiological complexities of antibiotic lethality. *Annu Rev Pharmacol Toxicol* **55**, 313-332 (2015).

37. Dwyer, D.J., *et al.* Antibiotics induce redox-related physiological alterations as part of their lethality. *Proc Natl Acad Sci U S A* **111**, E2100-2109 (2014).
38. Kanehisa, M. & Goto, S. KEGG: kyoto encyclopedia of genes and genomes. *Nucleic Acids Res* **28**, 27-30 (2000).
39. Bailey, T.L., *et al.* MEME SUITE: tools for motif discovery and searching. *Nucleic Acids Res* **37**, W202-208 (2009).
40. Dorr, T., *et al.* Differential requirement for PBP1a and PBP1b in in vivo and in vitro fitness of Vibrio cholerae. *Infect Immun* **82**, 2115-2124 (2014).
41. Dorr, T., *et al.* A novel peptidoglycan binding protein crucial for PBP1A-mediated cell wall biogenesis in Vibrio cholerae. *PLoS Genet* **10**, e1004433 (2014).
42. Ruiz, N. Lipid Flippases for Bacterial Peptidoglycan Biosynthesis. *Lipid Insights* **8**, 21-31 (2015).
43. Teo, A.C. & Roper, D.I. Core Steps of Membrane-Bound Peptidoglycan Biosynthesis: Recent Advances, Insight and Opportunities. *Antibiotics (Basel)* **4**, 495-520 (2015).
44. Davies, B.W., Bogard, R.W. & Mekalanos, J.J. Mapping the regulon of Vibrio cholerae ferric uptake regulator expands its known network of gene regulation. *Proc Natl Acad Sci U S A* **108**, 12467-12472 (2011).
45. White, J.R. & Yeowell, H.N. Iron enhances the bactericidal action of streptonigrin. *Biochem Biophys Res Commun* **106**, 407-411 (1982).
46. Yeowell, H.N. & White, J.R. Iron requirement in the bactericidal mechanism of streptonigrin. *Antimicrob Agents Chemother* **22**, 961-968 (1982).
47. Imlay, J.A. The molecular mechanisms and physiological consequences of oxidative stress: lessons from a model bacterium. *Nat Rev Microbiol* **11**, 443-454 (2013).
48. Imlay, J.A. The mismetallation of enzymes during oxidative stress. *J Biol Chem* **289**, 28121-28128 (2014).
49. Xia, X., *et al.* OxyR-activated expression of Dps is important for Vibrio cholerae oxidative stress resistance and pathogenesis. *PLoS One* **12**, e0171201 (2017).
50. Wang, H., *et al.* Catalases promote resistance of oxidative stress in Vibrio cholerae. *PLoS One* **7**, e53383 (2012).
51. Wang, H., *et al.* OxyR2 Modulates OxyR1 Activity and Vibrio cholerae Oxidative Stress Response. *Infect Immun* **85**(2017).
52. Storz, G., Tartaglia, L.A. & Ames, B.N. The OxyR regulon. *Antonie Van Leeuwenhoek* **58**, 157-161 (1990).
53. Johnson, L.A. & Hug, L.A. Distribution of reactive oxygen species defense mechanisms across domain bacteria. *Free Radic Biol Med* (2019).
54. Muras, V., Dogaru-Kinn, P., Minato, Y., Hase, C.C. & Steuber, J. The Na+-Translocating NADH:Quinone Oxidoreductase Enhances Oxidative Stress in the Cytoplasm of Vibrio cholerae. *J Bacteriol* **198**, 2307-2317 (2016).
55. Steuber, J., *et al.* The structure of Na(+)-translocating of NADH:ubiquinone oxidoreductase of Vibrio cholerae: implications on coupling between electron transfer and Na(+) transport. *Biol Chem* **396**, 1015-1030 (2015).
56. Tuomanen, E., Cozens, R., Tosch, W., Zak, O. & Tomasz, A. The rate of killing of Escherichia coli by beta-lactam antibiotics is strictly proportional to the rate of bacterial growth. *J Gen Microbiol* **132**, 1297-1304 (1986).

57. Weaver, A.I., *et al.* Genetic Determinants of Penicillin Tolerance in Vibrio cholerae. *Antimicrob Agents Chemother* **62**(2018).
58. Fillat, M.F. The FUR (ferric uptake regulator) superfamily: diversity and versatility of key transcriptional regulators. *Arch Biochem Biophys* **546**, 41-52 (2014).
59. Lee, J.W. & Helmann, J.D. The PerR transcription factor senses H2O2 by metal-catalysed histidine oxidation. *Nature* **440**, 363-367 (2006).
60. Helmann, J.D., *et al.* The global transcriptional response of Bacillus subtilis to peroxide stress is coordinated by three transcription factors. *J Bacteriol* **185**, 243-253 (2003).
61. Faulkner, M.J. & Helmann, J.D. Peroxide stress elicits adaptive changes in bacterial metal ion homeostasis. *Antioxid Redox Signal* **15**, 175-189 (2011).
62. Duarte, V. & Latour, J.M. PerR vs OhrR: selective peroxide sensing in Bacillus subtilis. *Mol Biosyst* **6**, 316-323 (2010).
63. Varghese, S., Wu, A., Park, S., Imlay, K.R. & Imlay, J.A. Submicromolar hydrogen peroxide disrupts the ability of Fur protein to control free-iron levels in Escherichia coli. *Mol Microbiol* **64**, 822-830 (2007).
64. Seo, S.W., *et al.* Deciphering Fur transcriptional regulatory network highlights its complex role beyond iron metabolism in Escherichia coli. *Nat Commun* **5**, 4910 (2014).
65. Masse, E. & Gottesman, S. A small RNA regulates the expression of genes involved in iron metabolism in Escherichia coli. *Proc Natl Acad Sci U S A* **99**, 4620-4625 (2002).
66. Kehres, D.G., Janakiraman, A., Slauch, J.M. & Maguire, M.E. Regulation of Salmonella enterica serovar Typhimurium mntH transcription by H(2)O(2), Fe(2+), and Mn(2+). *J Bacteriol* **184**, 3151-3158 (2002).
67. Martin, J.E., Waters, L.S., Storz, G. & Imlay, J.A. The Escherichia coli small protein MntS and exporter MntP optimize the intracellular concentration of manganese. *PLoS Genet* **11**, e1004977 (2015).
68. Ikeda, J.S., Janakiraman, A., Kehres, D.G., Maguire, M.E. & Slauch, J.M. Transcriptional regulation of sitABCD of Salmonella enterica serovar Typhimurium by MntR and Fur. *J Bacteriol* **187**, 912-922 (2005).
69. Fisher, C.R., Wyckoff, E.E., Peng, E.D. & Payne, S.M. Identification and Characterization of a Putative Manganese Export Protein in Vibrio cholerae. *J Bacteriol* **198**, 2810-2817 (2016).
70. Kawai, Y., *et al.* Cell growth of wall-free L-form bacteria is limited by oxidative damage. *Curr Biol* **25**, 1613-1618 (2015).
71. Kawai, Y., *et al.* Crucial role for central carbon metabolism in the bacterial L-form switch and killing by beta-lactam antibiotics. *Nat Microbiol* (2019).
72. Schnell, S. & Steinman, H.M. Function and stationary-phase induction of periplasmic copper-zinc superoxide dismutase and catalase/peroxidase in Caulobacter crescentus. *J Bacteriol* **177**, 5924-5929 (1995).
73. Longo, V.D., Gralla, E.B. & Valentine, J.S. Superoxide dismutase activity is essential for stationary phase survival in Saccharomyces cerevisiae. Mitochondrial production of toxic oxygen species in vivo. *J Biol Chem* **271**, 12275-12280 (1996).

74. Gort, A.S., Ferber, D.M. & Imlay, J.A. The regulation and role of the periplasmic copper, zinc superoxide dismutase of Escherichia coli. *Mol Microbiol* **32**, 179-191 (1999).
75. Martins, D.*, et al.* Superoxide dismutase activity confers (p)ppGpp-mediated antibiotic tolerance to stationary-phase Pseudomonas aeruginosa. *Proc Natl Acad Sci U S A* **115**, 9797-9802 (2018).
76. Haugan, M.S., Charbon, G., Frimodt-Moller, N. & Lobner-Olesen, A. Chromosome replication as a measure of bacterial growth rate during Escherichia coli infection in the mouse peritonitis model. *Sci Rep* **8**, 14961 (2018).
77. Keren, I., Kaldalu, N., Spoering, A., Wang, Y. & Lewis, K. Persister cells and tolerance to antimicrobials. *FEMS Microbiol Lett* **230**, 13-18 (2004).
78. Sharma, B., Brown, A.V., Matluck, N.E., Hu, L.T. & Lewis, K. Borrelia burgdorferi, the Causative Agent of Lyme Disease, Forms Drug-Tolerant Persister Cells. *Antimicrob Agents Chemother* **59**, 4616-4624 (2015).
79. Brynildsen, M.P., Winkler, J.A., Spina, C.S., MacDonald, I.C. & Collins, J.J. Potentiating antibacterial activity by predictably enhancing endogenous microbial ROS production. *Nat Biotechnol* **31**, 160-165 (2013).
80. Gutierrez, A.*, et al.* beta-Lactam antibiotics promote bacterial mutagenesis via an RpoS-mediated reduction in replication fidelity. *Nat Commun* **4**, 1610 (2013).
81. Sheldon, J.R. & Skaar, E.P. Metals as phagocyte antimicrobial effectors. *Curr Opin Immunol* **60**, 1-9 (2019).
82. Yang, J.H.*, et al.* A White-Box Machine Learning Approach for Revealing Antibiotic Mechanisms of Action. *Cell* **177**, 1649-1661 e1649 (2019).
83. Radlinski, L. & Conlon, B.P. Antibiotic efficacy in the complex infection environment. *Curr Opin Microbiol* **42**, 19-24 (2018).
84. Yang, J.H., Bening, S.C. & Collins, J.J. Antibiotic efficacy-context matters. *Curr Opin Microbiol* **39**, 73-80 (2017).
85. Stokes, J.M., Lopatkin, A.J., Lobritz, M.A. & Collins, J.J. Bacterial Metabolism and Antibiotic Efficacy. *Cell Metab* (2019).
86. Donnenberg, M.S. & Kaper, J.B. Construction of an eae deletion mutant of enteropathogenic Escherichia coli by using a positive-selection suicide vector. *Infect Immun* **59**, 4310-4317 (1991).
87. Dalia, A.B. Natural Cotransformation and Multiplex Genome Editing by Natural Transformation (MuGENT) of Vibrio cholerae. *Methods Mol Biol* **1839**, 53-64 (2018).
88. Hubbard, T.P.*, et al.* A live vaccine rapidly protects against cholera in an infant rabbit model. *Sci Transl Med* **10**(2018).
89. Gibson, D.G.*, et al.* Enzymatic assembly of DNA molecules up to several hundred kilobases. *Nat Methods* **6**, 343-345 (2009).
90. Dorr, T., Cava, F., Lam, H., Davis, B.M. & Waldor, M.K. Substrate specificity of an elongation-specific peptidoglycan endopeptidase and its implications for cell wall architecture and growth of Vibrio cholerae. *Mol Microbiol* **89**, 949-962 (2013).
91. Beauchamp, C. & Fridovich, I. Superoxide dismutase: improved assays and an assay applicable to acrylamide gels. *Anal Biochem* **44**, 276-287 (1971).

Figure 1

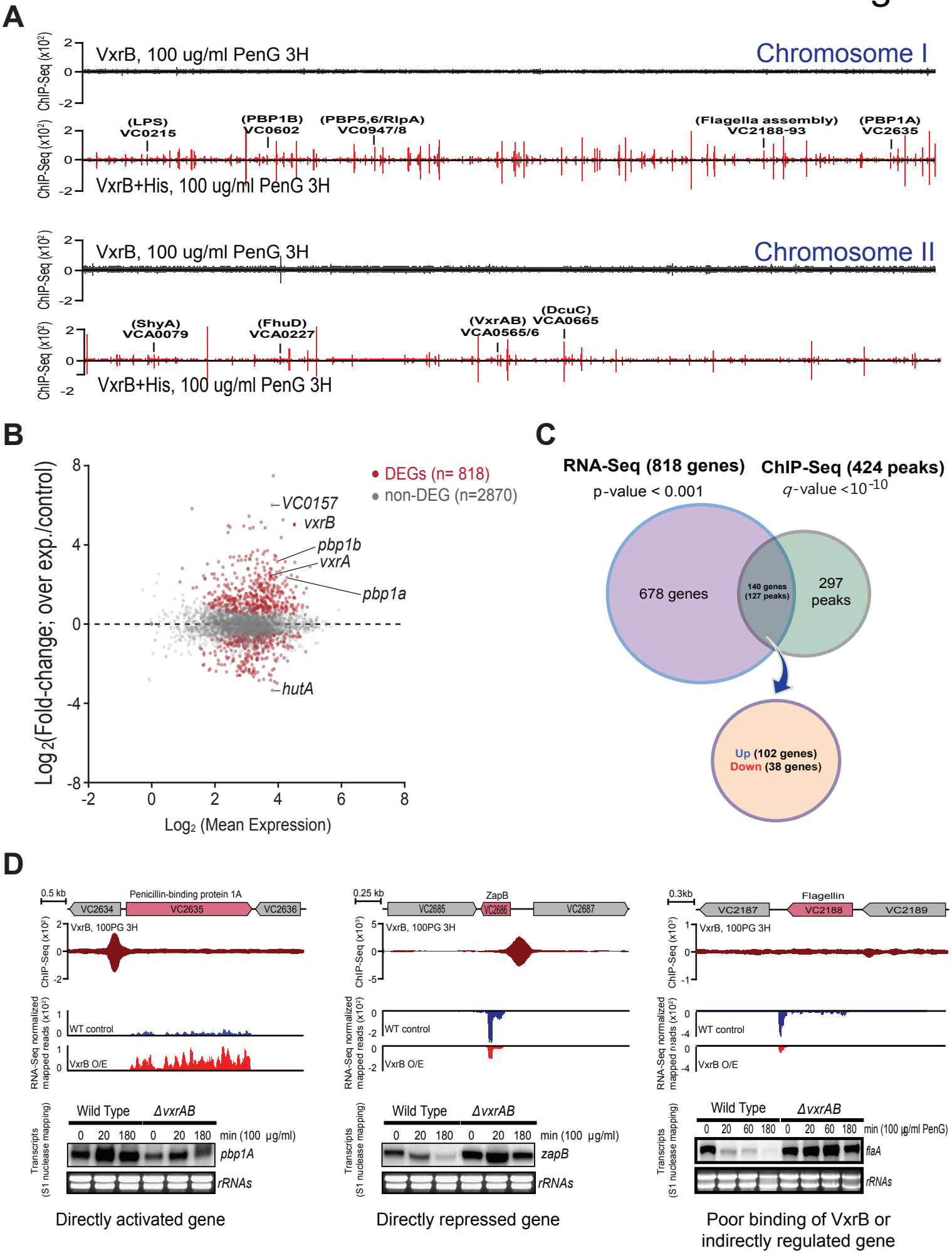
A
VxrB, 100 ug/ml PenG 3H
Chromosome I
ChIP-Seq (x10²)
(LPS) VC0215
(PBP1B) VC0602
(PBP5,6/RlpA) VC0947/8
(Flagella assembly) VC2188-93
(PBP1A) VC2635
VxrB+His, 100 ug/ml PenG 3H
VxrB, 100 ug/ml PenG 3H
Chromosome II
(ShyA) VCA0079
(FhuD) VCA0227
(VxrAB) VCA0565/6
(DcuC) VCA0665
VxrB+His, 100 ug/ml PenG 3H
B
DEGs (n= 818)
non-DEG (n=2870)
VC0157
vxrB
pbp1b
vxrA
pbp1a
hutA
Log2(Fold-change; over exp./control)
Log2 (Mean Expression)
C
RNA-Seq (818 genes)
p-value < 0.001
ChIP-Seq (424 peaks)
q-value <10-10
678 genes
140 genes (127 peaks)
297 peaks
Up (102 genes)
Down (38 genes)
D
0.5 kb
Penicillin-binding protein 1A
VC2634
VC2635
VC2636
VxrB, 100PG 3H
ChIP-Seq (x10²)
RNA-Seq normalized mapped reads (x10²)
WT control
VxrB O/E
Transcripts (S1 nuclease mapping)
Wild Type
ΔvxrAB
0 20 180 0 20 180 min (100 µg/ml)
pbp1A
rRNAs
Directly activated gene
0.25 kb
ZapB
VC2685
VC2686
VC2687
VxrB, 100PG 3H
ChIP-Seq (x10³)
WT control
VxrB O/E
Wild Type
ΔvxrAB
0 20 180 0 20 180 min (100 µg/ml)
zapB
rRNAs
Directly repressed gene
0.3kb
Flagellin
VC2187
VC2188
VC2189
VxrB, 100PG 3H
ChIP-Seq (x10³)
WT control
VxrB O/E
Wild Type
ΔvxrAB
0 20 60 180 0 20 60 180 min (100 µg/ml PenG)
flaA
rRNAs
Poor binding of VxrB or indirectly regulated gene

Figure 2

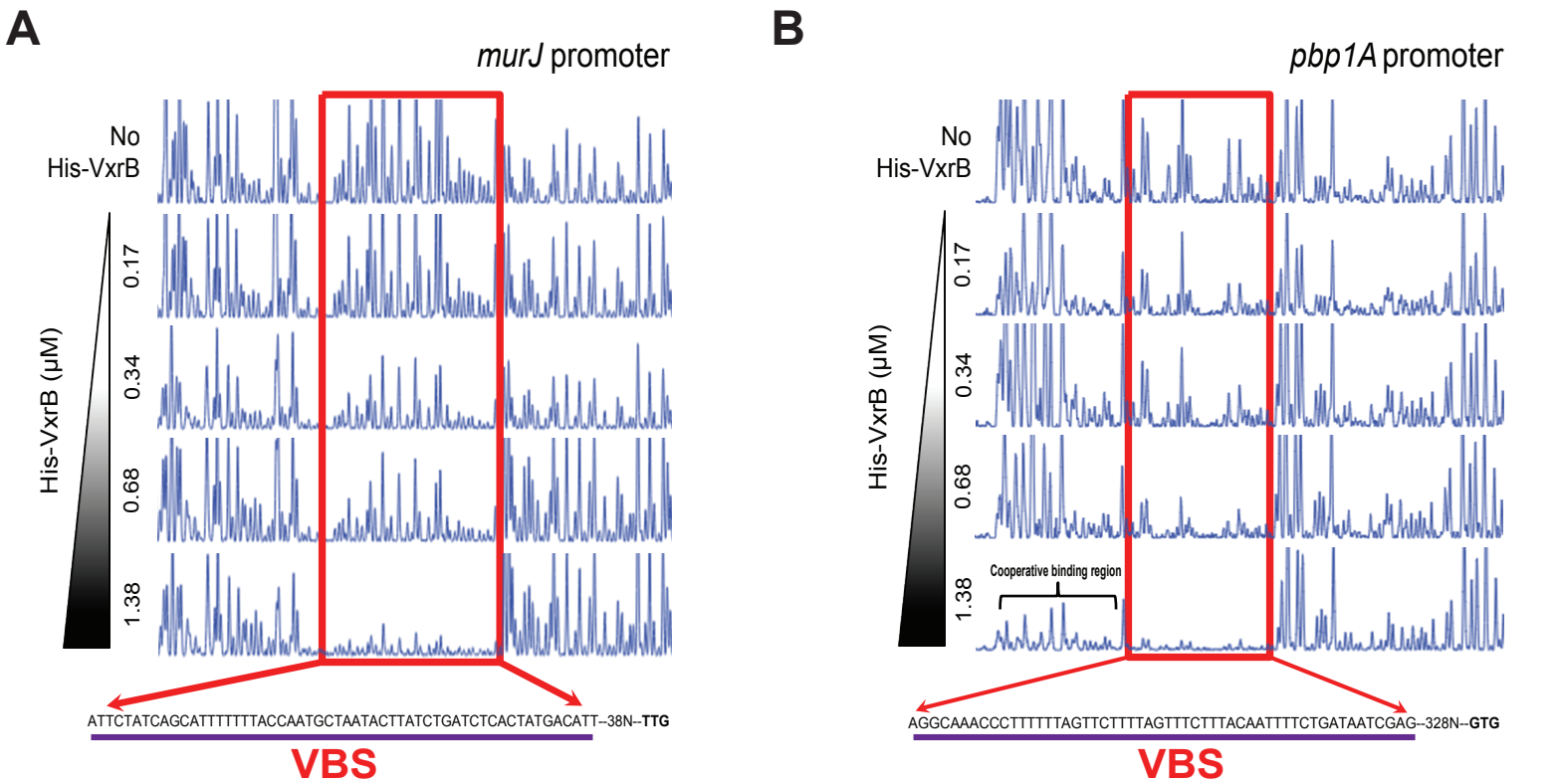
A
murJ promoter
No His-VxrB
His-VxrB (μM)
0.17
0.34
0.68
1.38
ATTCTATCAGCATTTTTTTACCAATGCTAATACTTATCTGATCTCACTATGACATT--38N--TTG
VBS
B
pbp1A promoter
No His-VxrB
His-VxrB (μM)
0.17
0.34
0.68
1.38
Cooperative binding region
AGGCAAACCCTTTTTTAGTTCTTTTAGTTTCTTTACAATTTTCTGATAATCGAG--328N--GTG
VBS

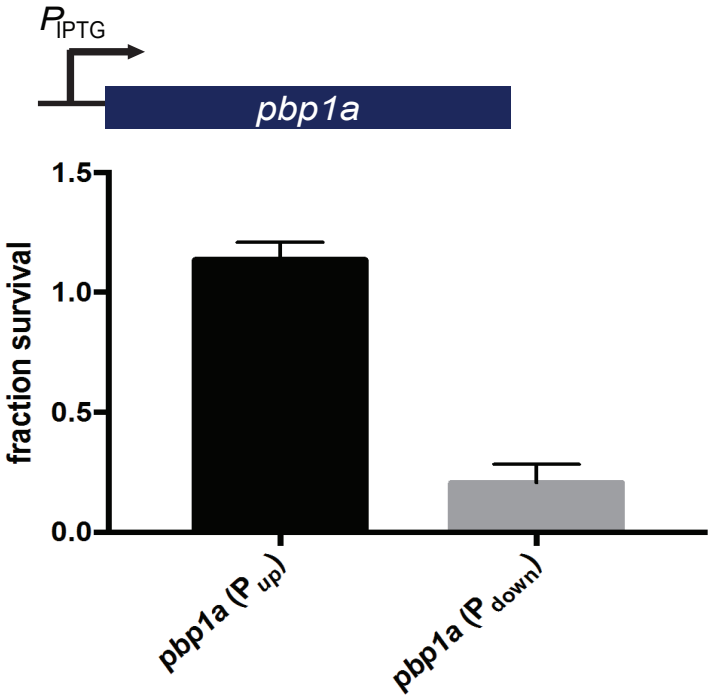
C
P_{IPTG}
pbp1a
fraction survival
1.5
1.0
0.5
0.0
pbp1a (P_{up})
pbp1a (P_{down})

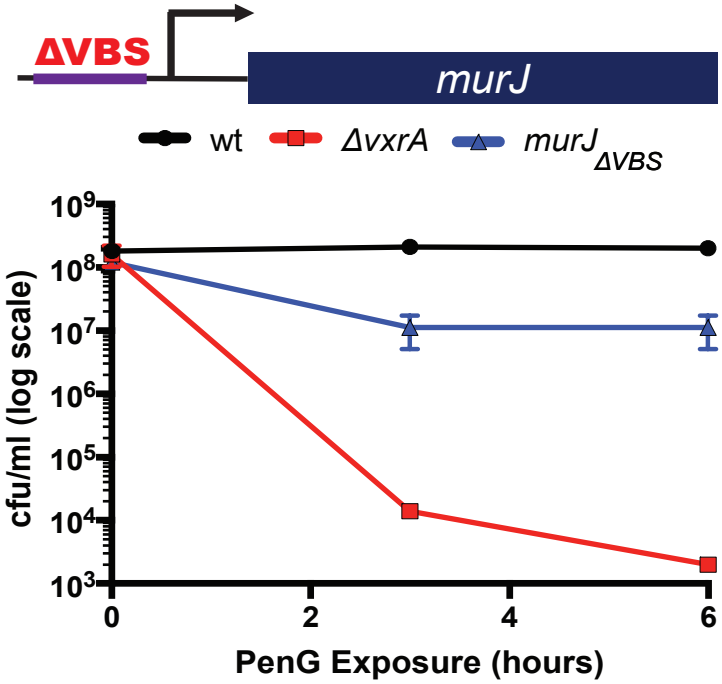
E
ΔVBS
murJ
wt
ΔvxrA
murJ ΔVBS
cfu/ml (log scale)
10^9
10^8
10^7
10^6
10^5
10^4
10^3
0
2
4
6
PenG Exposure (hours)

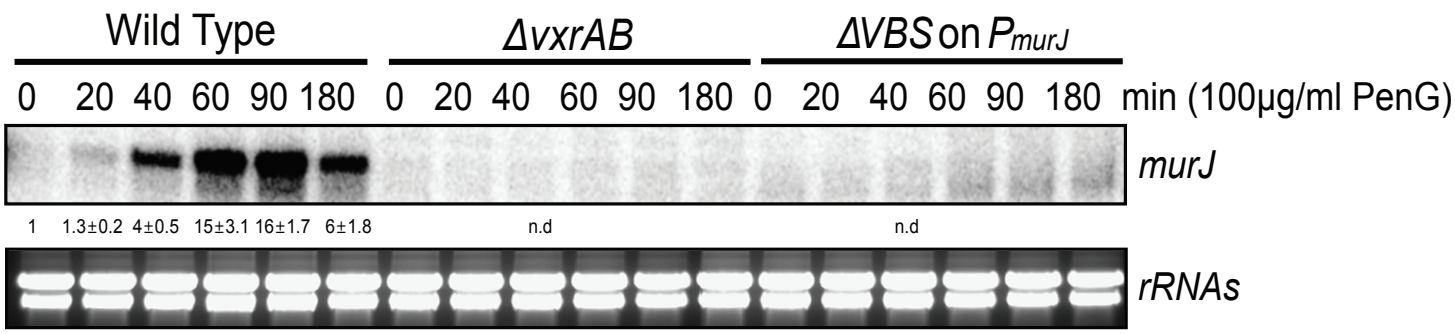
D
Wild Type
ΔvxrAB
ΔVBS on P_{murJ}
0 20 40 60 90 180 0 20 40 60 90 180 0 20 40 60 90 180 min (100μg/ml PenG)
murJ
1 1.3±0.2 4±0.5 15±3.1 16±1.7 6±1.8
n.d
n.d
rRNAs

Figure 3

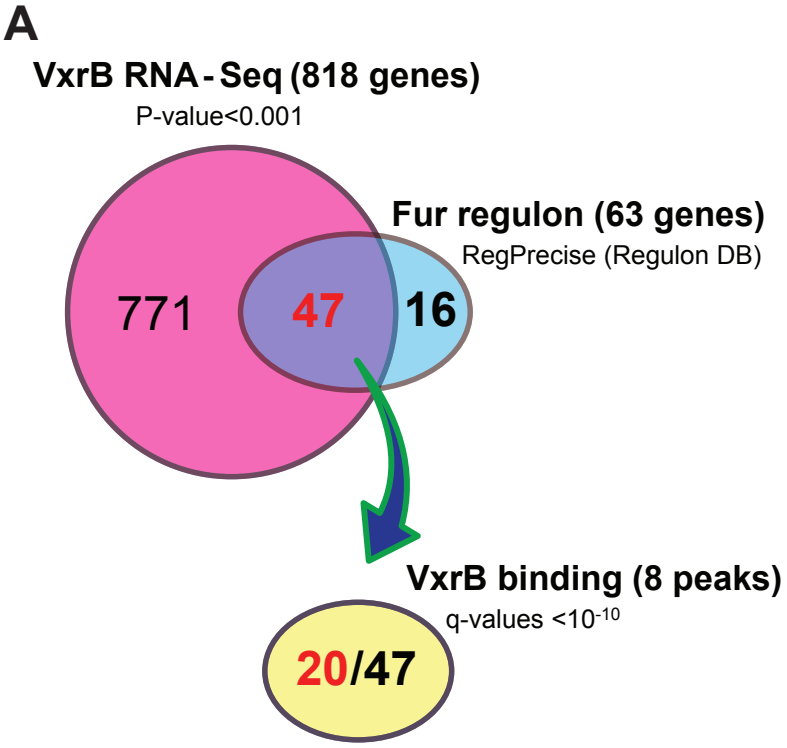
A
VxrB RNA-Seq (818 genes)
P-value<0.001
771
47
16
Fur regulon (63 genes)
RegPrecise (Regulon DB)
VxrB binding (8 peaks)
q-values <10-10
20/47

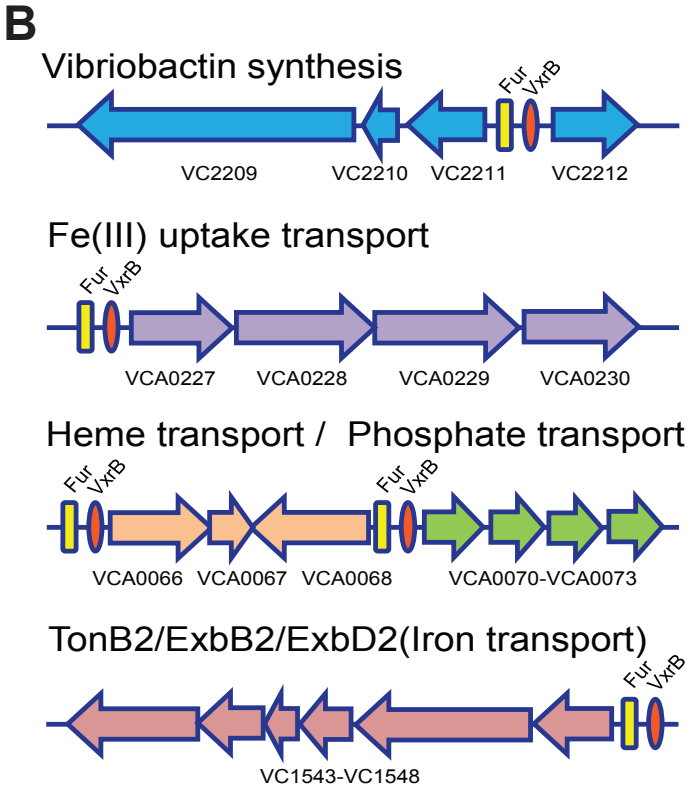
B
Vibriobactin synthesis
Fur
VxrB
VC2209
VC2210
VC2211
VC2212
Fe(III) uptake transport
VCA0227
VCA0228
VCA0229
VCA0230
Heme transport / Phosphate transport
VCA0066
VCA0067
VCA0068
VCA0070-VCA0073
TonB2/ExbB2/ExbD2(Iron transport)
VC1543-VC1548

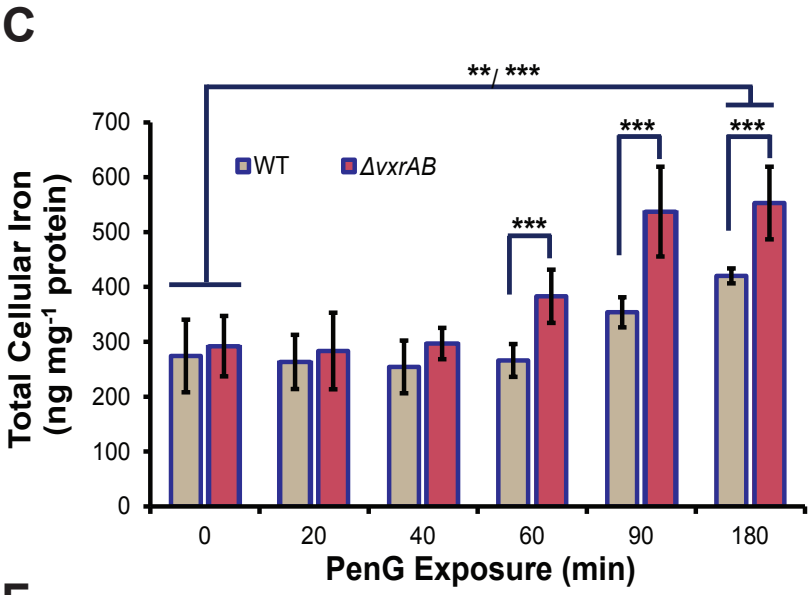
C
/ *
***
***
***
WT
ΔvxrAB
Total Cellular Iron (ng mg-1 protein)
700
600
500
400
300
200
100
0
0
20
40
60
90
180
PenG Exposure (min)

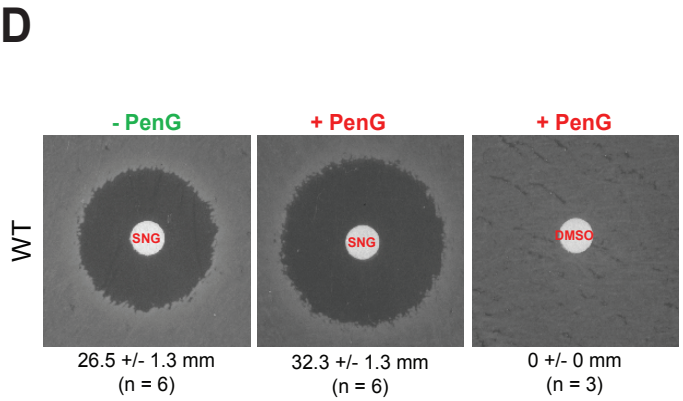
D
- PenG
+ PenG
+ PenG
WT
SNG
SNG
DMSO
26.5 +/- 1.3 mm
(n = 6)
32.3 +/- 1.3 mm
(n = 6)
0 +/- 0 mm
(n = 3)

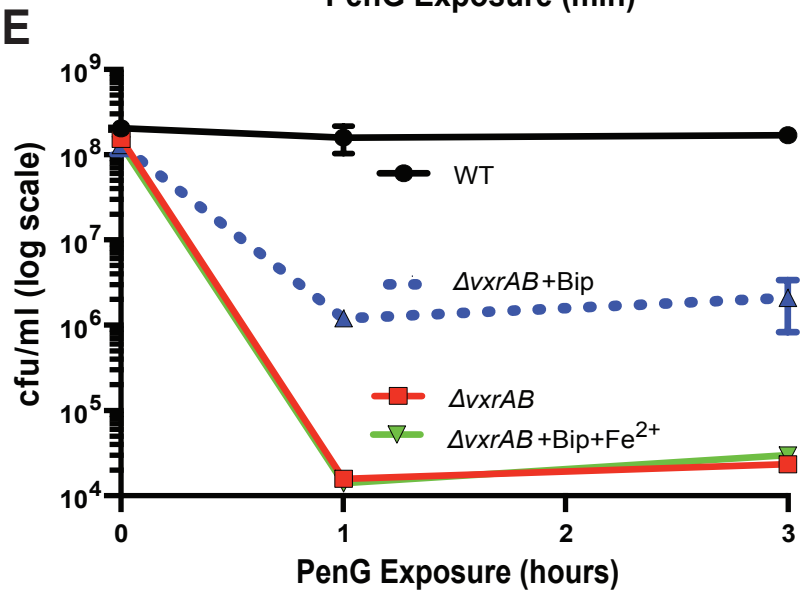
E
cfu/ml (log scale)
10^9
10^8
10^7
10^6
10^5
10^4
WT
ΔvxrAB+Bip
ΔvxrAB
ΔvxrAB+Bip+Fe2+
0
1
2
3
PenG Exposure (hours)

Figure 4

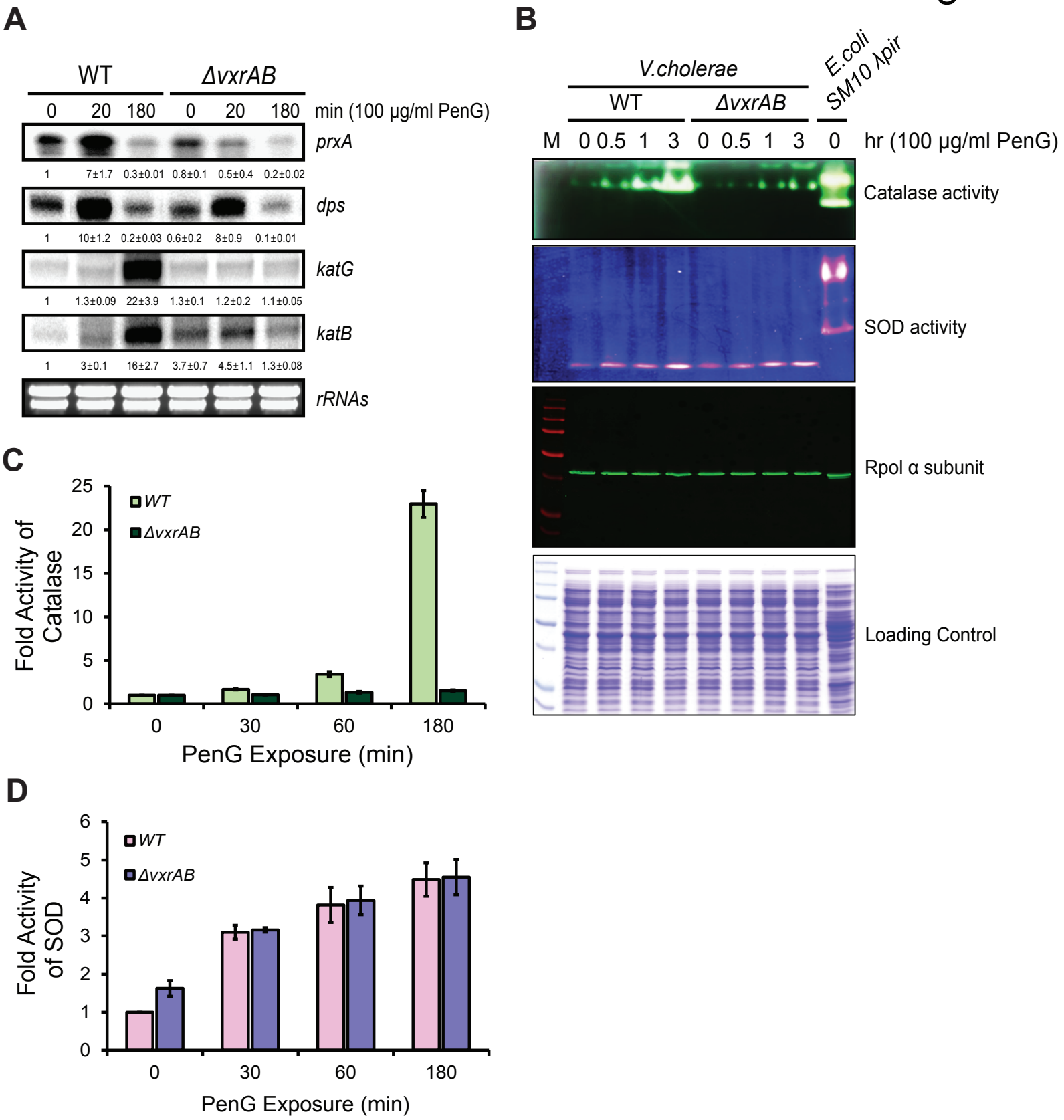
A
WT
ΔvxrAB
0 20 180 0 20 180 min (100 μg/ml PenG)
prxA
1 7±1.7 0.3±0.01 0.8±0.1 0.5±0.4 0.2±0.02
dps
1 10±1.2 0.2±0.03 0.6±0.2 8±0.9 0.1±0.01
katG
1 1.3±0.09 22±3.9 1.3±0.1 1.2±0.2 1.1±0.05
katB
1 3±0.1 16±2.7 3.7±0.7 4.5±1.1 1.3±0.08
rRNAs
B
V.cholerae
E.coli SM10 λpir
WT
ΔvxrAB
M 0 0.5 1 3 0 0.5 1 3 0 hr (100 μg/ml PenG)
Catalase activity
SOD activity
Rpol α subunit
Loading Control
C
Fold Activity of Catalase
WT
ΔvxrAB
0 30 60 180
PenG Exposure (min)
D
Fold Activity of SOD
WT
ΔvxrAB
0 30 60 180
PenG Exposure (min)

Figure 5

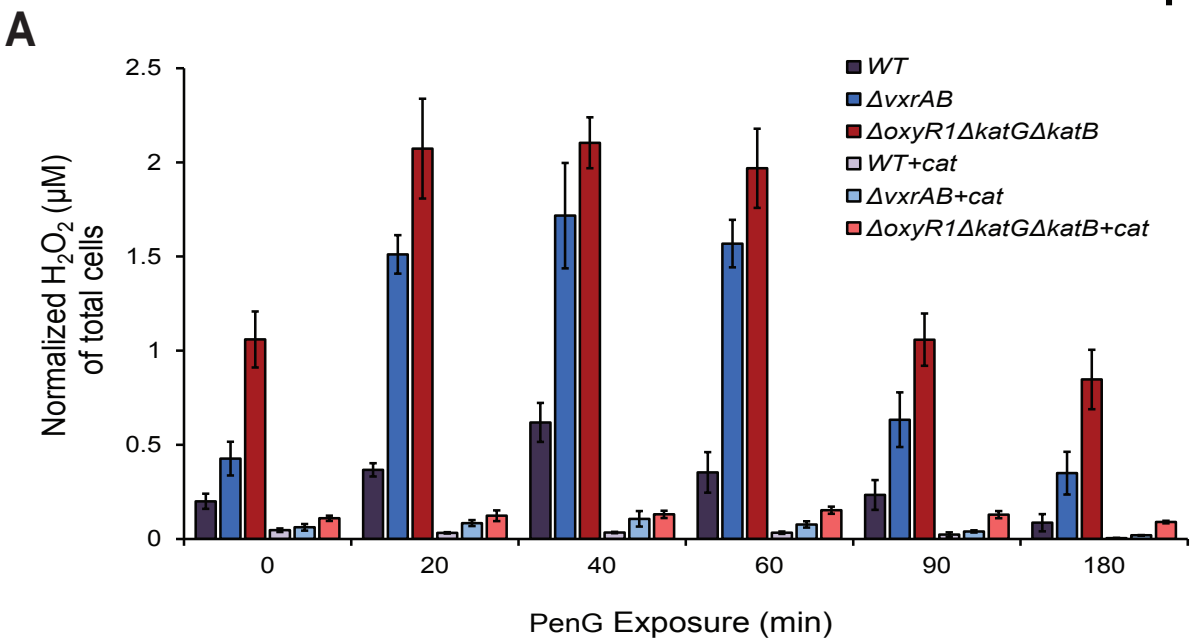
A
Normalized H_2O_2 (μM) of total cells
2.5
2
1.5
1
0.5
0
WT
ΔvxrAB
ΔoxyR1ΔkatGΔkatB
WT+cat
ΔvxrAB+cat
ΔoxyR1ΔkatGΔkatB+cat
0
20
40
60
90
180
PenG Exposure (min)

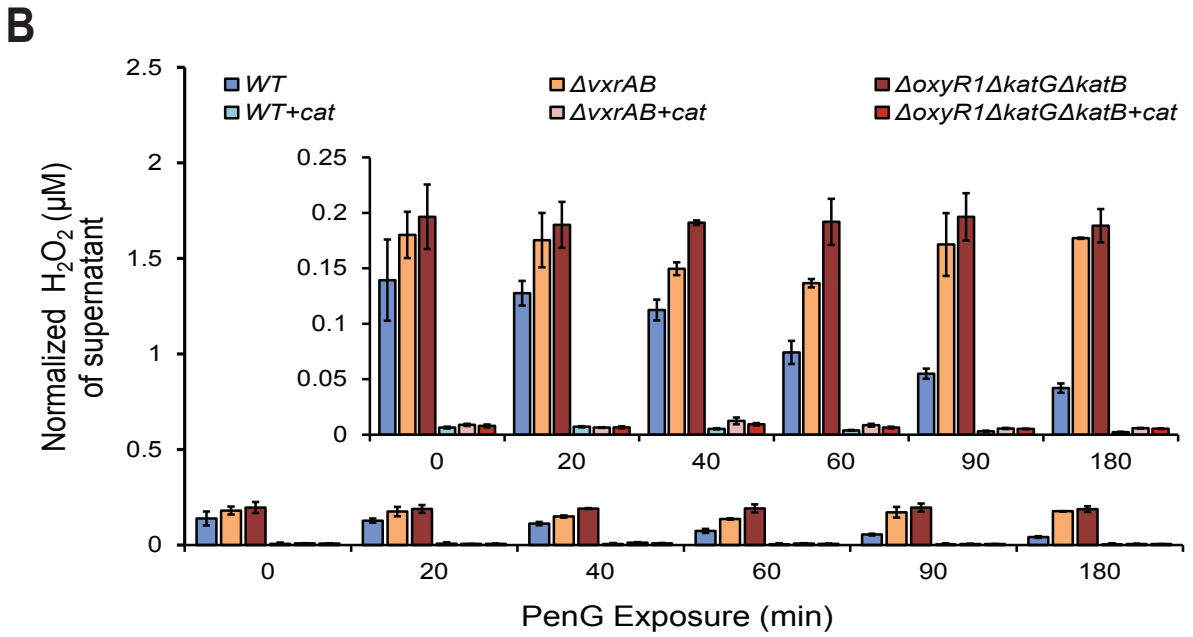
B
Normalized H_2O_2 (μM) of supernatant
2.5
2
1.5
1
0.5
0
WT
WT+cat
ΔvxrAB
ΔvxrAB+cat
ΔoxyR1ΔkatGΔkatB
ΔoxyR1ΔkatGΔkatB+cat
0.25
0.2
0.15
0.1
0.05
0
0
20
40
60
90
180
PenG Exposure (min)

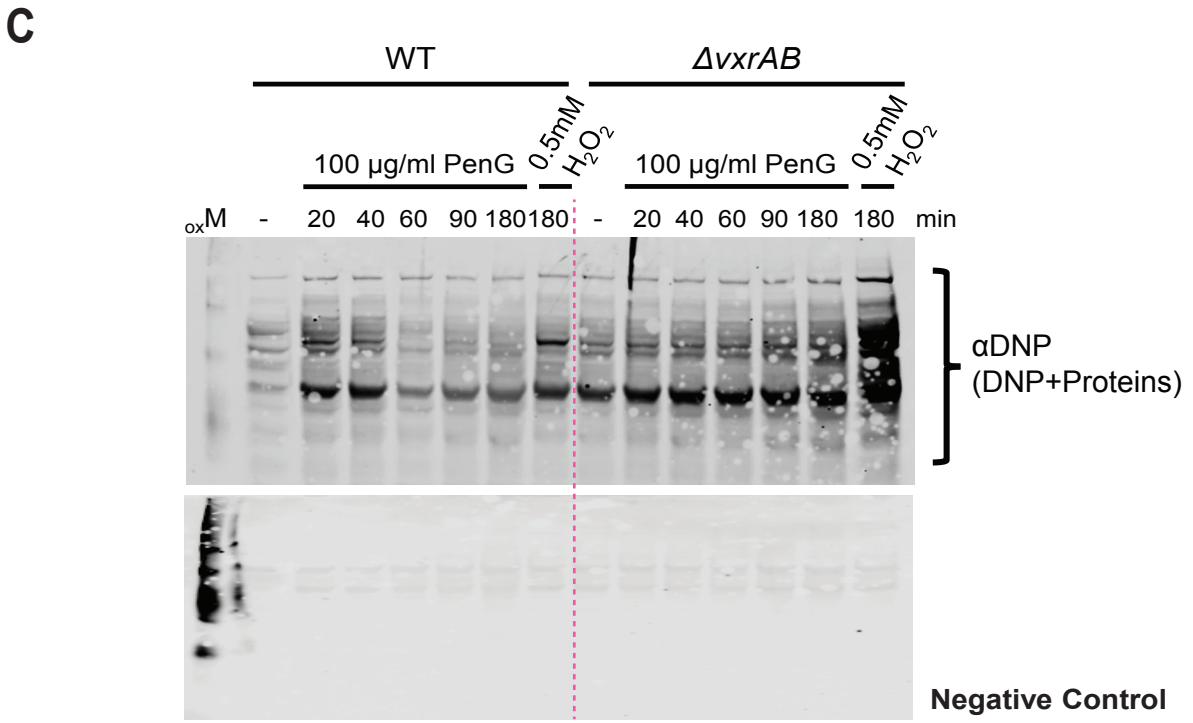
C
WT
ΔvxrAB
100 μg/ml PenG
0.5mM H_2O_2
100 μg/ml PenG
0.5mM H_2O_2
oxM
-
20
40
60
90
180
180
-
20
40
60
90
180
180
min
αDNP
(DNP+Proteins)
Negative Control

Figure 6

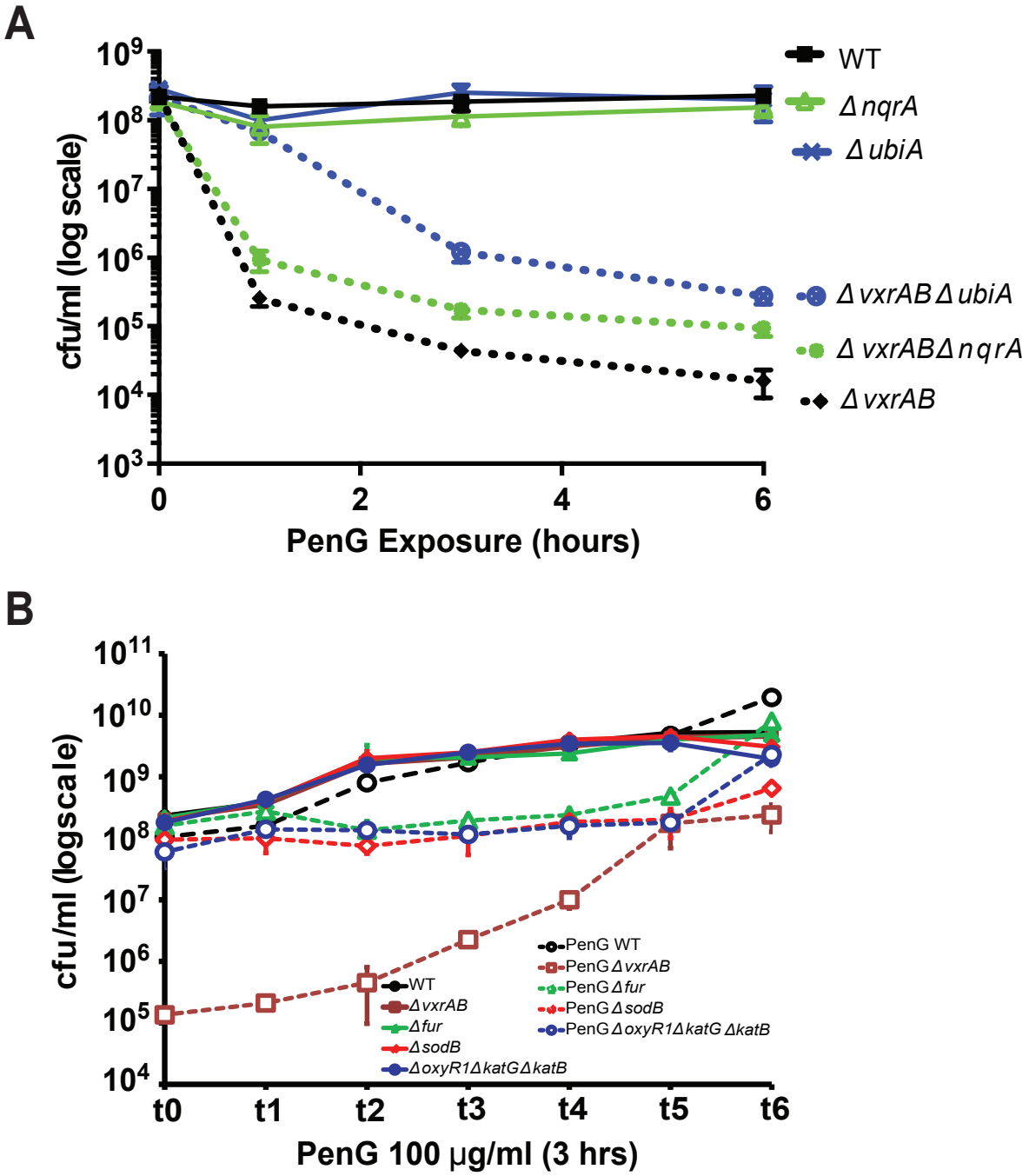
A
cfu/ml (log scale)
PenG Exposure (hours)
WT
ΔnqrA
ΔubiA
ΔvxrABΔubiA
ΔvxrABΔnqrA
ΔvxrAB
B
cfu/ml (logscale)
PenG 100 µg/ml (3 hrs)
WT
ΔvxrAB
Δfur
ΔsodB
ΔoxyR1ΔkatGΔkatB
PenG WT
PenGΔvxrAB
PenGΔfur
PenGΔsodB
PenGΔoxyR1ΔkatGΔkatB

Figure 7

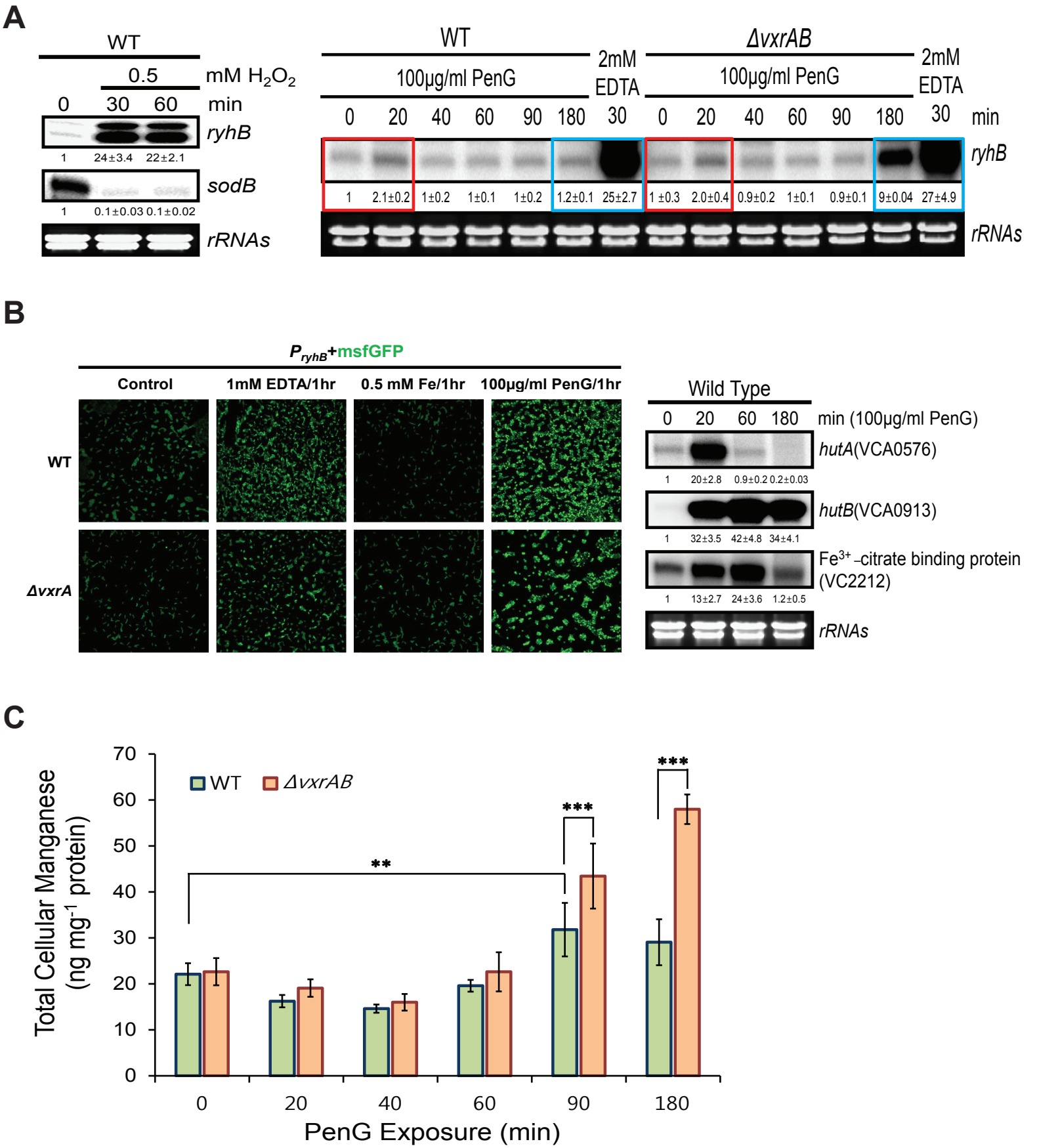
A
WT
0.5
mM H2O2
0 30 60 min
ryhB
1 24±3.4 22±2.1
sodB
1 0.1±0.03 0.1±0.02
rRNAs
WT
100μg/ml PenG
2mM EDTA
0 20 40 60 90 180 30 min
1 2.1±0.2 1±0.2 1±0.1 1±0.2 1.2±0.1 25±2.7
ΔvxrAB
100μg/ml PenG
2mM EDTA
0 20 40 60 90 180 30 min
1 ±0.3 2.0±0.4 0.9±0.2 1±0.1 0.9±0.1 9±0.04 27±4.9
ryhB
rRNAs
B
PryhB+msfGFP
Control
1mM EDTA/1hr
0.5 mM Fe/1hr
100μg/ml PenG/1hr
WT
ΔvxrA
Wild Type
0 20 60 180 min (100μg/ml PenG)
hutA(VCA0576)
1 20±2.8 0.9±0.2 0.2±0.03
hutB(VCA0913)
1 32±3.5 42±4.8 34±4.1
Fe3+-citrate binding protein (VC2212)
1 13±2.7 24±3.6 1.2±0.5
rRNAs
C
Total Cellular Manganese (ng mg-1 protein)
WT
ΔvxrAB
**
***
***
0
10
20
30
40
50
60
70
0 20 40 60 90 180
PenG Exposure (min)